1 **Advancement toward coupling of the VAMPER permafrost model within the earth system**
2 **model *i*LOVECLIM (version 1.0): description and validation**

3 D. Kitover, R. van Balen, D.M. Roche, J. Vandenberghe, H. Renssen

4 Earth and Climate Cluster, Faculty of Earth and Life Sciences, Vrije Universiteit Amsterdam, Amsterdam,
5 the Netherlands

6 Correspondence to: D.C. Kitover (d.c.kitover@vu.nl)

7 **Abstract**

8 The VAMPER permafrost model has been enhanced with snow thickness and active layer calculations in
9 preparation for coupling within the *i*LOVECLIM earth system model of intermediate complexity. In
10 addition, maps of basal heat flux and lithology were developed within ECBilt, the atmosphere
11 component of *i*LOVECLIM, so that VAMPER may use spatially varying parameters of geothermal heat flux
12 and porosity values. The enhanced VAMPER model is validated by comparing the simulated modern day
13 extent of permafrost thickness with observations. To perform the simulations, the VAMPER model is
14 forced by *i*LOVECLIM land surface temperatures. Results show that the simulation which did not include
15 the snow cover option overestimated the present permafrost extent. However, when the snow
16 component is included, the simulated permafrost extent is reduced too much. In analyzing simulated
17 permafrost depths, it was found that most of the modeled thickness values and subsurface
18 temperatures fall within a reasonable range of the corresponding observed values. Discrepancies
19 between simulated and observed are due to lack of captured effects from features such as topography
20 and organic soil layers. In addition, some discrepancy is also due to disequilibrium with the current
21 climate, meaning that some permafrost is a result of colder states and therefore cannot be reproduced
22 accurately with the *i*LOVECLIM preindustrial forcings.

23

24 **1   Introduction**

25 The **VU Am**sterdam **Per**mafrost (VAMPER) model is a deep 1-d heat conduction model with phase
26 change capability. It has been previously validated for single site experiments such as Barrow, Alaska
27 (Kitover et al., 2012). Subsequently, it has simulated both equilibrium and transient permafrost depth
28 estimates at a number of arctic/subarctic locations (Kitover et al., 2012; Kitover et al., 2013). The
29 VAMPER model was built with the intention to couple it within *i*LOVECLIM, an earth system model of
30 intermediate complexity. Using this coupling, the goal is to capture the transient nature of permafrost
31 growth/decay over millennia as a feedback effect during major periods of climate change. To prepare for
32 coupling, a few enhancements have since been made to the VAMPER model. As a next step, we validate
33 these improvements by simulating modern-day permafrost thickness and distribution. The goal of this
34 paper is to describe the enhancements and then analyze the validation experiments for modeling
35 present-day permafrost, with detailed explanation of why mismatches occur between simulated and
36 observed data.

1   The first example of VAMPER as a stand-alone deep permafrost model was for Barrow, Alaska (Kitover
2   et al., 2012) where the experiment reproduced the present-day permafrost depth using monthly
3   averaged observation data of ground "surface" (- 1 cm deep) temperatures. In this same study,
4   VAMPER was also validated by comparing results against other developed deep permafrost models (also
5   used for millennial-scale simulations) using similar forcings and parameter settings. In both Kitover et al.
6   (2012) and Kitover et al. (2013), a number of transient simulations at selected locations (e.g. Wyoming,
7   West Siberia, Central Siberia) were performed using the stand-alone version of the VAMPER model,
8   forced by *i*LOVECLIM-generated land surface temperatures over the last 21k years (Roche et al., 2011).
9   In addition, a sensitivity analysis was presented in Kitover et al. (2013), showing the range of simulated
10   permafrost depths under different parameter settings.

11   Thus far, according to the work summarized above, VAMPER has only been employed as a site-specific
12   permafrost model. However, the advantage of the model being simple with limited parameterization
13   requirements, hence resulting in speedy computation times, have not been fully realized since it is not
14   yet coupled within *i*LOVECLIM. As a next step, this paper describes the necessary developments and
15   validation to couple VAMPER with ECBilt, the atmospheric component of *i*LOVECLIM. Specifically, this
16   presented work introduces two enhancements to the VAMPER model : 1) inclusion of snow as optional
17   layers and 2) change in the timestep. The first in particular is an issue in modeling permafrost since snow
18   cover is a recognized influence on the ground thermal regime (Williams and Smith, 1989) and was not an
19   available option in the previous VAMPER model version. To compensate for this, Kitover et al. (2013)
20   had artificially introduced the effect of snow cover via a surface offset (the difference between the
21   ECBilt land surface temperature and the VAMPER ground surface temperature) of + 2°C. Not only was
22   this an assumption based on a number of previous reports and observations, but it had to be applied as
23   an annual surface offset since the time step was one year. This then demonstrates the need for the
24   other enhancement, which is a sub-annual timestep, where the seasonal changes in the ground thermal
25   conditions can be captured, allowing for representation of both the snow cover effect and the active
26   layer. In addition to the VAMPER model enhancements, two global maps were produced (geo-processed
27   from the original maps to fit the horizontal grid of ECBilt) to be used as additional input parameters to
28   the VAMPER model: geothermal heat flux and porosity. These are particularly used when VAMPER is
29   run over a horizontal grid, in turn allowing the parameters to vary spatially.

30   Integrating permafrost into earth system models has become of increased interest since research has
31   acknowledged the effect of climate change on permafrost temperatures (Cheng and Wu, 2007),
32   permafrost degradation (Anisimov and Nelson, 1996), and carbon stored within the permafrost
33   (Davidson and Janssens, 1996). The Coupled Model Intercomparison Project phase 5 (Koven et al.,
34   2013) analyzed how different earth system models represent the subsurface thermal dynamics and how
35   well this class of models simulate permafrost and active layer depth. Despite the fact that there is a
36   variety of modeling methods and configurations for the different global coupled models, the conclusion
37   was that there is no clear ranking among the reviewed 15+ model versions. This shows that
38   representing permafrost in earth system models still has some challenges, which Koven et al. (2013)
39   attribute primarily to modeling of both the atmosphere/ground energy exchange and the subsurface
40   thermal regime. Until recently, most simulations of permafrost were calibrated for regional or local

1 study such as Li and Koike (2003) on the Tibetan Plateau, Zhang et al. (2006) in Canada, and Nicolsky et
2 al. (2009) in Alaska. A growing number of studies are now modeling permafrost across the Northern
3 Hemisphere or globally. Simulations are done using either statistical approaches like the frost index
4 method (Anisimov and Nelson, 1996; Stendel and Christensen,2002) or climate models such as Dankers
5 et al., (2011) who used the JULES land surface model and Ekici et al. (2014) who used the JSBACH
6 terrestrial ecosystem model. Other examples include Lawrence and Slater (2005), who used the
7 Community Climate System Model (CCSM) to look at future permafrost extent and associated changes
8 in freshwater discharge to the Arctic Ocean. Schaeffer et al. (2011) used a land surface model (SiBCASA)
9 to simulate reduced future permafrost coverage and subsequent magnitude of the carbon feedback.
10 Similarly, Schneider von Deimling et al.(2012) and Koven et al. (2011) also modeled future estimates of
11 carbon emissions due to thawing permafrost. From a paleoclimate perspective, DeConto et al. (2012)
12 used a version of the GENESIS GCM to model the connection between permafrost degradation and
13 subsequent carbon emission as a driver for the occurrence of the Palaeocene–Eocene Thermal
14 Maximum (PETM). Modeling permafrost changes is also an interest from the hydrological perspective.
15 Avis et al. (2011) used a version of the UVic Earth System Climate Model to examine the potential
16 decreasing areal extent of wetlands due to future permafrost thaw.

17 However, it should be noted that there is a difference between coupled models which actively integrate
18 the role of permafrost (including the thermal, hydrological, and/or carbon feedbacks) (Lawrence et al.,
19 2011), and models which look at permafrost in a post-processing perspective (e.g. Buteau et al., 2004,
20 Ling and Zhang, 2004)meaning they are forced by the predicted temperature changes. It is the full
21 coupling with integrated feedbacks which is of our current interest, where the goal is to fully couple
22 ECBilt and VAMPERS within *i*LOVECLIM. The results of the work presented here serve as an important
23 validation stage toward this goal. In the sections following, the two enhancements to the VAMPER
24 model are explained. This includes validation of the timestep change by comparing simulated annual
25 active layer depths with empirical-based estimates. Next, two newly developed maps of spatially varying
26 parameters used in the VAMPER experiments are explained. For the validation, the VAMPER model is
27 forced by ECBilt land surface temperatures, where the results are compared against a modern-day map
28 of permafrost extent in the northern hemisphere and observed permafrost thickness and subsurface
29 temperatures values in boreholes.

30

31 **2   METHODS**

32 **2.1   VAMPER model**

33 **2.1.1.   General Description**

34 VAMPER is a 1-d permafrost model developed to estimate permafrost thickness and is designed for
35 eventual full coupling with *i*LOVECLIM. Consequently, the representation of the soil and subsurface in
36 VAMPER should fit the spatial space of *i*LOVECLIM, implying that detailed parameterization schemes are
37 not suitable for VAMPER.VAMPER is meant rather as a generalized model to simulate conceptual
38 permafrost thickness based on the factors which most strongly dictate the subsurface thermal regime.

1 Most notable for our purposes and discussed by Farouki (1981), these factors are mineral composition,
2 water content, and temperature.

3 Other than what is specified below, construction of the VAMPER model has not changed and the
4 methods as described in Kitover et al., (2013) still apply. In particular, these include assuming only
5 conductive heat transfer in the subsurface and employing well-established methods for finding the
6 temperature-dependent thermal properties of heat capacity and thermal conductivity (Farouki, 1981;
7 Zhang et al., 2008). The subsurface is assumed to be saturated (i.e. porosity equals the water content)
8 and there is currently no groundwater flow either horizontally or vertically between the soil layers.

9 The phase change process of freeze/thaw in the subsurface is handled using a modified apparent heat
10 capacity method from Mottaghy and Rath (2006). Their method assumes that phase change occurs
11 continuously over a temperature range, which in our case is approximately between 0 and -2 °C. The
12 apparent heat capacity method includes an additional latent heat term in the heat diffusivity equation
13 as a way to account for the added energy released (consumed) during freeze (thaw) of the subsurface
14 water content. The latent heat demand during phase change, referred to as the 'zero curtain effect',
15 slows thermal diffusivity rates near the surface as the active layer freezes and thaws but also during
16 permafrost degradation/aggradation.

17

18 **2.1.2   VAMPER Model Enhancements**

19 As compared to most permafrost modeling studies, there are few which have reproduced changes in
20 permafrost thickness over geologic time periods. In these cases, they assume a larger timestep in their
21 numerical simulations (usually one month or one year) (e.g., Osterkamp and Gosink, 1991; Lebret et al.,
22 1994; Lunardini, 1995; Delisle, 1998) since they only need to force the models with the low frequency
23 changes in air temperature or ground temperature that occur over millennia. At this timescale, it is not
24 necessary to use a sub-annual timestep. In our earlier work with the VAMPER model (Kitover et al.,
25 2013), we similarly used a yearly timestep. However, in light of the future coupling between ECBilt and
26 VAMPER, it has become clear that the VAMPER model should run on a 4-hr timestep. Doing this allows
27 VAMPER to match the timescale of the atmosphere, the subsystem to which the VAMPER model will be
28 coupled. Changing to a 4-hour timestep also reduces error in the numerical approximation since the
29 change in thermal properties, which are temperature-dependent, is smoother between each timestep.
30 Since the VAMPER model is somewhat simplified, and hence flexible, the change to a 4-hr timestep
31 required revalidating the model performance. In addition to the change in timestep, we also included a
32 snowpack representation in the VAMPER model. Including this option is meant to simulate the effect of
33 thermal insulation of the ground in winter. *Note that the VAMPER model with the snow enhancement is*
34 *referred to as the VAMPER**S** model. When referring to both/either versions, the "VAMPER(S)" term is*
35 *used.*

36 *Timestep*

1 To illustrate the difference between applying the same annual average temperature forcing but with
2 two different timesteps (4-hr vs. yearly), a sensitivity test was performed (**Fig. 1a**). To generate the sub-
3 daily surface temperature forcing (4 hours), a year-long temperature time-series was calculated using a
4 standard sine function with constant amplitude 20°C and average annual temperature of -6 °C
5 (hereafter referred to as sensitivity run 1 or "sr1"), resulting in an annual range of temperatures
6 between -26 °C and 14°C. The case with a yearly timestep, called "sr2", used -6 °C as the constant
7 forcing. Besides the change in timestep and corresponding surface temperature forcing, the thermal
8 conductivity and heat capacity values were also allowed to differ since these variables are temperature-
9 dependent (**Fig. 1b**). However, the lower boundary heat flux and porosity parameter settings were the
10 same in both model runs. Each experiment was run until approximate equilibrium was reached under
11 the same constant (respective) forcing. We consider equilibrium to be when the geothermal heat flux is
12 approximately equal to the ground heat flux (what goes in = what goes out). Comparing the final depth-
13 temperature profiles between sr1 and sr2 shows a shift in the equilibrium depth-temperature profile
14 where using an annual timestep underestimates permafrost thickness by approximately 50 meters (**Fig.**
15 **1a**). This difference is attributed to occurrence of the thermal offset (difference between ground
16 temperature and top of the permafrost) within the active layer in sr1 (**Fig. 1b**), whereas sr2 cannot
17 exhibit such seasonal phenomena. Since VAMPER is a simple model (absence of vegetation, organics, an
18 unsaturated subsurface, or temporally varying water content) we can attribute the thermal offset to
19 seasonal differences in thermal conductivity, whereas the thermal conductivity of ice is four times that
20 of unfrozen water and therefore the freezing front is propagated more effectively than the warming
21 front. This difference causes the mean annual subsurface temperature within the active layer to be
22 gradually colder with depth. The offset is visible in the mean annual depth-temperature profile within
23 the top meter of **Figure 1b**.

24 *Active Layer*

25 In permafrost modeling, an active layer can only be present when the air/ground temperature forcing
26 varies seasonally. Thus, the timestep must be sub-annual. Since a 4-hr timestep is now implemented,
27 the VAMPER model produces an active layer. It necessary within the framework of model development
28 to then check the simulation of this active layer for validation purposes.

29 Most dynamical permafrost models that simulate near-surface behavior configure the parameter
30 settings to specifically match locally observed data. Some parameterizations include organic and mineral
31 layer thicknesses, which give soil properties such as porosity and bulk density, and unfrozen water
32 content characteristics. Examples of these site-specific studies include for example, Romanovsky and
33 Osterkamp (2000), Buteau et al. (2004), Ling and Zhang (2004), and Zhang et al.(2008), and Nicolsky et al
34 (2009). Since VAMPER is not parameterized to capture site-specific behavior, it is challenging to assess
35 the ability of the model to simulate active layer dynamics. Fortunately, there is a calculation called the
36 Stefan equation, used originally in engineering applications (Fox et al., 1992), to estimate the thickness
37 of the active layer when the amount of energy input and thermal characteristics are known. From
38 French (2007), the Stefan equation is defined as

39 $AL = \sqrt{2\sigma k_{mw}/Q_i}$ (1)

1   where AL (m) is the thickness of the active layer, σ is the cumulative thawing index (average ground
2   surface temperature (°C) during the thaw season times the duration of thaw season (s)), and k_{mw} is the
3   thermal conductivity of unfrozen soil (W (m K)$^{-1}$). Q_i (J m^{-3}) is defined further as

4    $$Q_i = L\rho_m(W - W_u)$$ (2)

5   where L is the latent heat of fusion, ρ_m is the dry density of the soil (kg m^{-3}), W is the total moisture
6   content , and W_u is the unfrozen water content . **Table 1** gives the constant variable values applied in the
7   Stefan Equation, which are the same values used in a comparable run for the VAMPER model

8   Under different forcings as a function of both average annual ground surface temperature and annual
9   amplitude, the VAMPER model's active layer thickness versus results using the Stefan Equation are
10   shown in **Table 2**. It is clear when comparing the empirically-based results with the series of simulations,
11   that the VAMPER model does a suitable job of reproducing annual active layer thickness.

12   ***Snowpack parameterization***

13   An additional option to the VAMPER model is the ability to extend the heat conduction model into the
14   snowpack when present. Prior to this, the surface offset, illustrated in Smith and Riseborough (2002),
15   could not be produced in the VAMPER model.

16   The VAMPERS model uses snow water equivalent (swe) values (m) with corresponding density to
17   compute snow thickness layers. Snow water equivalent is the depth of water that would result from the
18   complete melting of snow. The precipitation simulated in ECBilt is computed from the precipitable water
19   of the first atmospheric layer (Goosse et al., 2010). When the air temperature is below 0 °C, the
20   precipitation is assumed to be snow. However, this 'snow' is only assumed to be frozen water, meaning
21   it lacks any quantifiable properties besides the actual precipitation amount, and as such is directly
22   considered the swe value. As a result, there is an additional set of necessary functions when coupled
23   with VAMPERS to transfer ECBilt swe values into a snowpack thickness (Z) at time t:

24   $$Z^t = \rho_w\, swe^t / \rho_s^t$$ (3)

25   where ρ_w is water density and ρ_s snow density (Lynch-Stieglitz, 1994). The total snow density is
26   determined as a combination of old snow (expressed as swe^{t-1} from the previous timestep) and freshly
27   fallen snow at current timestep (expressed as swe^{fr}) :

28   $$\rho_s^t = \left.\left(swe^{t-1}\, \rho_s^{t-1} + swe^{fr}\, \rho_{fr}\right)\middle/ swe^t\right.$$ (4)

29   $$swe^t = swe^{t-1} + swe^{fr}$$ (5)

30   where ρ_{fr} is the density of fresh snow (150 kg m^{-3}).

31   There is snowpack metamorphism that occurs from a number of different processes. Notably, Dingman
32   (2002) distinguishes these as gravitational settling, destructive metamorphism, constructive

1   metamorphism, and melt. However, as these different changes occur at highly varying rates and under

2   localized conditions (aspect, slope, vegetation cover), it is impossible to incorporate such processes in an

3   Earth System Model of Intermediate Complexity (EMIC) such as *i*LOVECLIM. On the other hand, a

4   snowpack always undergoes densification over time and this effect should somehow be applied to the

5   modeled snowpack. Therefore, we apply to the total snow density an empirical densification function

6   due to mechanical compaction. The maximum allowable density is 500 kg m^{-3}, which cannot hold any

7   more liquid water (Dingman, 2002). The compaction equation used (e.g. Pitman et al.,1991; Lynch-

8   Stieglitz, 1994;) is as follows:

9    $$\rho_s^t = \rho_s^{t-1} + \left(0.5 \times 10^7 \rho_s^{t-1} \; g \; N \; \exp\left[14.643 - \frac{4000}{\min(T+273.16\,,273.16)} - 0.02\rho_s^{t-1}\right]\right)\Delta t \qquad (6)$$

10   where *g* is gravity (9.82 m s^{-2}), *N* (kg) is the mass of half the snowpack, *T* (°C) is the temperature of the

11   snowpack (the average temperature of the snow layer temperatures from the previous timestep), and

12   *Δt* is the timestep (*s*).

13   Three snow layers are then discretized from the total snow thickness, depending on whether it is above

14   or below 0.2 m, as outlined in Lynch-Stieglitz (1994). Thermal properties are then calculated for each

15   snow layer based on empirical formulas :

16   $K_S = 2.9 \, \rho_s{}^2$ (Goodrich, 1982)   (7)

17   $C_S = 1.9 \times 10^6 \rho_s/\rho_f$ (Verseghy, 1991)   (8)

18   where K_s is the snow thermal conductivity and C_s is the snow heat capacity, and ρ_f is the density of ice

19   (920 kg m^{-3}). All three snow layers are subject to the same processes and simply depend on

20   temperature, time, and thickness for their respective deformation and/or melting.

21   The following is a stepped description of the snow algorithm to generate a VAMPERS snowpack from

22   ECBilt precipitation:

23   1. Calculate new snow density, Eq. (4) and Eq. (5), using any freshly fallen snow and old snow.

24   2. Apply compaction function, Eq. (6) to snowpack.

25   3. Calculate total snow thickness using Eq. (3).

26   4. Discretize the individual layer thicknesses based on total snow thickness.

27   5. Calculate thermal properties for each layer (Eq. (7) and Eq. (8)).

28   6. Use snow thicknesses and corresponding thermal properties as additional layers in the

29   VAMPERS model.

30

31   **2.2   *i*LOVECLIM v 1.0**

32   **2.2.1   General Description**

33   *i*LOVECLIM is a "code-fork" of LOVECLIM 1.2 (Goosse et al., 2010), both which belong to a class of

34   climate models called EMICs (Claussen et al., 2002). This type of model, as summarized by Weber

35   (2010), "describes the dynamics of the atmosphere and/or ocean in less detail than conventional

1 General Circulation Models". This simplification reduces computation time, thus making EMICs suitable
2 for simulations on millennial timescales, incorporating the components with slow feedback effects, such
3 as icesheets, vegetation, and permafrost. Different versions of LOVECLIM have successfully simulated
4 past climates including the LGM (Roche et al., 2007), the Holocene (Renssen et al., 2005, 2009), and the
5 last millennium (Goosse et al., 2005). Although there exist some different developments between
6 *i*LOVECLIM and the LOVECLIM versions, both consist of the following coupled earth system
7 components: the atmosphere (ECBilt), the ocean (CLIO), and vegetation (VECODE) (**Fig. 2**). ECBilt, the
8 atmospheric model (Opsteegh et al., 1998) consists of a dynamical core with three vertical levels at 800,
9 500, and 200 hPa. It runs on a spectral grid with a triangular T21 truncation, which translates to a
10 horizontal grid with a resolution of approximately 5.6 ° lat x 5.6 ° lon. The CLIO module (Goosse and
11 Fichefet, 1999) is a 3-D ocean general circulation model with a free surface. It has 3° × 3° horizontal
12 resolution and 20 vertical layers. VECODE, the vegetation module (Brovkin et al., 1997), is similar to
13 VAMPER(S) in that it was particularly designed for coupling to a coarse-resolution earth system model. It
14 is a reduced-form dynamic global vegetation model that characterizes the land surface as either trees,
15 grass, or no vegetation (i.e. 'bare soil') and is computed at the same resolution as ECBilt. The plant types
16 may be represented fractionally within each gridcell. Each model component of *i*LOVECLIM was
17 originally developed separately and the reader is referred to Goosse et al., 2010 for a detailed
18 description of components and coupling mechanisms. Furthermore, *i*LOVECLIM more recently was
19 extended with other optional components including the dynamical ice-sheet model GRISLI (Roche et al.,
20 2014) and a stable water isotopes scheme (Roche, 2013).

21 **2.2.2   ECBilt-VAMPER(S) Coupling Description**

22 The VAMPER(S) model will be coupled to the atmospheric component, ECBilt, within *i*LOVECLIM. The
23 ECBilt-VAMPER(S) coupling will be done at each timestep (4 hours) where the land surface temperature
24 from ECBilt is passed to VAMPER(S) and the ground heat flux from VAMPER(S) is returned to ECBilt (Fig.
25 3a). The land surface temperature is calculated within ECBilt as a function of the heat balance equation
26 where the major heat fluxes across the air/surface interface are incorporated: sensible heat flux, latent
27 heat flux, shortwave radiation, longwave radiation, and ground heat flux. The land surface temperature
28 and ground heat flux are only communicated between components when the respective grid cell is
29 classified as land with no overlying icesheet (i.e. Greenland/Antarctica at present day). With this
30 coupling, the effect of changing permafrost conditions may be reflected in the climate via changes in the
31 surface energy balance. If permafrost degrades, the subsurface acts as a thermal sink, absorbing
32 additional energy to accommodate latent heat demands during phase change. However, at the same
33 time, the active layer deepens, also redistributing the (seasonal) energy distribution at the surface.

34 When only VAMPER is employed, i.e. without the snowpack, the VAMPER ground surface temperature is
35 assumed to be the same as the ECBilt land surface temperature. As a result no surface offset occurs. In
36 the case of VAMPERS the snow surface temperature (i.e. at the top of the snow layer) is assumed to be
37 the same as the ECBilt land surface temperature. This means the VAMPERS model ground temperature
38 is buffered via the three snowpack layers as discussed in Sect. 2.1.2. This description is illustrated in
39 Figure 3b. The ground surface temperature is the forcing that the VAMPER(S) model then uses to
40 compute the subsurface temperature profile. This calculation, via the implicitly solved heat equation

1 with phase change capability, is fully described in Kitover et al. (2013). As VAMPER is a 1-D model, there

2 is no lateral energy (heat/water) transfer between adjacent grid cells in the subsurface. Permafrost

3 thickness is determined at an annual timestep using a computed average annual temperature profile,

4 where any depth below or equal to 0°C is considered permafrost. Although in reality there is a freezing

5 point depression which may occur as a result of the local pressure or dissolved salts, we are consistent

6 with the thermal definition of permafrost from the International Permafrost Association: "ground (soil

7 or rock and included ice or organic material) that remains at or below 0°C for at least two consecutive

8 years".

9 The land surface of ECBilt consists of a single "layer" which represents a volumetric soil water storage

10 capacity to generate surface runoff when full. This system is referred to as a bucket model in previous

11 text (Goosse et al., 2010). As of current, this hydrology portion of ECBilt, will not be coupled to

12 VAMPERS. However, because the active layer is a regulator of hydrology in arctic and subarctic regions

13 (Hinzman and Kane, 1992; Genxu et al., 2009), a next step would be to expand coupling between

14 VAMPERS and ECBilt by connecting the active layer with this bucket model.

15 The first phase of the coupling between VAMPERS and ECBilt will only include the land surface

16 temperature and the ground heat flux as discussed. It should be mentioned as a caveat that additional

17 coupling mechanisms are possible between *i*LOVECLIM components and VAMPER, which include

18 hydrology and the carbon cycle, but will not be implemented for the first coupling phase.

19 **2.2.3   Geothermal Heat Flux**

20 The VAMPER(S) model requires a geothermal heat flux as the lower surface boundary. In Kitover et al.

21 (2013), a sensitivity analysis was performed to look at the equilibrium permafrost thickness as a result of

22 varying the geothermal heat flux and found that thickness can increase by about 70 m with every

23 decrease in flux of 10 mW m^{-2}. To obtain the geothermal heat flux for every cell in the ECBilt grid, we

24 used the recent publication of Davies (2013) who determined the median of heat flux estimates per

25 approximately 2° x 2° latitude-longitude grid based on a combination of actual measurements,

26 modeling, and correlation assumptions. However, due to the mismatch of grid resolutions between

27 Davies (2013) and ECBilt, we determined for each ECBilt grid cell, a simple area-weighted average of the

28 Davies (2013) estimates. In other words, each of the Davies grid cells was assigned a weighing factor

29 based on the percentage of overlap with the ECBilt cells. Below is the original map from Davies (2013)

30 and the averaged map applied in the VAMPER(S) experiments (**Fig. 4**). A preliminary sensitivity analysis

31 between applying the geothermal heat flux map and applying the continental global average (approx. 60

32 mW m^{-2}) showed no noticeable difference in permafrost distribution. This result is different, however,

33 than the noticeable sensitivity of geothermal heat flux on permafrost depth (Kitover et al., 2013).

34

35 **2.2.4   Porosity**

36 Another variable needed to run the VAMPER(S) model is the porosity values throughout depth, which in

37 these experiments is down to 3000 meters deep. In previous VAMPER studies (Kitover et al., 2012;

1 Kitover et al., 2013), it was always assumed that the land subsurface was sedimentary rock, with a
2 porosity of 0.3, 0.4, or 0.5. However, as shown in Kitover et al. (2013), the porosity, or water content,
3 has a noticeable effect on equilibrium permafrost thickness. That sensitivity test showed about a 50 m
4 difference in permafrost thickness when the porosity values (assuming a saturated subsurface) ranged
5 between 0.3 and 0.5. Therefore, to both narrow our assumptions regarding the subsurface but still
6 maintain the simplification necessary for the coarse horizontal grid, an additional lithological
7 classification scheme was created as an additional VAMPER(S) model parameter. Using the recently
8 published Global Lithological Map Database (GLiM) from Hartmann and Moosdorf (2012), their original
9 seven categories were reclassified into 'Bedrock (Bed)' , (e.g., granitic and metamorphic rock), and
10 'Sedimentary (Sed)' (e.g., sandstone, limestone) (**Table 3, Fig. 5**). In the case of 'Bed', the subsurface
11 would presumably be quite consolidated/compressed, resulting in a low water content (Almén et al.,
12 1986; Gleeson et al., 2014). 'Bed' was thus assigned a low porosity of 0.1, which based on sources that
13 showed depth profiles of bedrock sites (Schild et al., 2001; Nováková et al., 2012), stayed constant with
14 depth. On the other hand, similar to the case studies from Kitover et al. (2013), a depth porosity
15 function from Athy (1930) was applied for the 'Sed' class, where the surface porosity (Φ) was assumed
16 to be 0.40 and a decay constant (4×10^{-4}) in the exponential equation, representing the average for
17 sandy textured soil. Similar to application of the geothermal heat flux map, a preliminary sensitivity
18 analysis between applying the lithology map and applying a constant value (0.4) throughout the globe
19 showed only marginal differences in permafrost distribution. This result is different, however, than the
20 higher sensitivity of porosity on permafrost depth (Kitover et al., 2013)

21

22 **3   Validation of preindustrial permafrost thickness distribution**

23 **3.1   Experimental Setup**

24 The model experiments are performed over the whole globe where the VAMPER model is forced by
25 ECBilt land surface temperatures. These values are the lower boundary layer of the atmosphere and are
26 calculated using a surface heat budget (Goosse et al., 2010). Referring to Figure 3a, this means that
27 ECBilt passes temperature values to the VAMPER(S) model (right side of **Fig. 3**) but no data is returned
28 to ECBilt (left side of **Fig. 3**), leaving the climate unaffected from permafrost or changes in permafrost.
29 The model experiments also include the spatially varying parameter values of geothermal heat flux and
30 porosity provided by the new maps (described in sections 2.2.3 and 2.2.4) . Two different model runs
31 were made: one without the snow enhancement or any imposed surface offset (VAMPER) and one with
32 the snow enhancement (VAMPERS). These two are first compared in sect. 3.2.1 of the Results &
33 Discussion below.

34 Because permafrost has a very slow thermal response (Lunardini, 1995) as compared to other
35 components in *i*LOVECLIM, VAMPER(S) is not forced synchronously by ECBilt. Rather, VAMPER(S) is
36 forced continuously for 100 years and then runs offline for 900 years using the ECBilt average land
37 surface temperature of the previous 100 years as the forcing. This asynchronous cycle is repeated for
38 thousands of years until the VAMPER(S) model is equilibrated to the (already) equilibrated *i*LOVECLIM

1   preindustrial climate. This scheme is illustrated in **Fig. 6** (adapted from a similar figure in McGuffie and

2   Henderson-Sellers (2005)). Equilibrium was determined when the lower boundary heat flux

3   approximately matches the annual average ground surface heat flux. This is also when the permafrost

4   thickness is stable. Although the model approaches a steady state through the subsurface depth, we

5   acknowledge that in reality, some of the permafrost regions are not at equilibrium since they are

6   responding to recent warming.

7   **3.2   Results and Discussion**

8   In order to verify the performance of VAMPER(S) forced by *i*LOVECLIM, a series of equilibrium

9   experiments were performed for the preindustrial (PI) climate (~ 1750 AD). For comparative purposes,

10 we assume the PI state of permafrost is similar enough to the current state of permafrost that we used

11 modern-day data to validate against the PI simulations. The simulated areal extent was compared to

12 present-day extent using the "Circumarctic Map of Permafrost and Ground-Ice Conditions" (Brown et

13 al., 2014). Unlike the model validation done by Lawrence and Slater (2005), and then subsequently

14 critiqued by Burn and Nelson (2006), our simulations attempt to capture the extent of both continuous

15 and discontinuous permafrost. In addition, available borehole data, for sites within the arctic/subarctic,

16 were used to evaluate the simulated thicknesses. Therefore, there are two types of validation

17 approaches: 1) permafrost distribution and 2) permafrost depth.

18 **3.2.1   Permafrost Distribution Validation**

19 The first validation demonstrates the extent to which the VAMPERS model reproduces the modern-day

20 permafrost distribution.   The results can be matched against a study comparing a suite of earth system

21 models, namely the Coupled Model Intercomparison Project phase 5 (CMIP5) (Koven et al., 2013). This

22 report gives the simulated preindustrial permafrost areas under a number of different earth system

23 climate models and configurations. Compared to the results from our study, some of the other models'

24 simulated permafrost distributions cover more area while some cover less. The maximum is reported as

25 28.6 x 10^6 km^2 and minimum 2.7 x 10^6 km^2. Our simulation using VAMPERS yields approximately 20.3 x

26 10^6 km^2 . This is a reasonably comparable estimate since almost 80 % (14/18) of the model area extents

27 from Koven et al. (2012) fall within ±40% (12 – 28 x 10^6 km^2) of our model estimate. According to

28 discussion by Koven et al., (2012), most of the variation seen among the compared earth system models

29 is primarily attributed to the subsurface modeling techniques, such as water content, using a latent heat

30 term, and differing soil thermal conductivities. Secondary causes are attributed to the air-ground

31 coupling such as incorporation of organics and a snowpack (bulk or multilayer). These conclusions are

32 not different from our own study in that 1) snowpack plays a marked role in permafrost modeling and

33 inclusion/exclusion will impact the results, 2) the air-ground coupling is also a source of potential

34 mismatch (discussed further in section 3.2.2).

35 Using the comparison shown in Figure 7, which overlays the simulated results on the map from Brown et

36 al. 2014., it is clear that the experiment without the snow option overestimates permafrost extent while

37 employing the VAMPER**S** version underestimates it. This inaccuracy between both an overestimated

38 result and an underestimated result is at least partially due to attempting to match results from a low

1   resolution grid to spatial coverage of much higher resolution. Because the marginal areas of permafrost

2   extent are the most sensitive to climate, they are highly responsive to minor temperature deviations.

3   These deviations, whether a few degrees above or below freezing, determine from a modeling point of

4   view, whether permafrost exists or not. In the case of VAMPER, average annual ground surface

5   temperatures in many of these marginal grid cells fall below freezing while in the case of VAMPERS, the

6   temperatures in these same grid cells now fall above freezing. However, because of the coarse grid,

7   these estimates in either case, look like inaccurate estimates since a single value is representative of a

8   relatively large spatial area. In reality, in these marginal permafrost regions, an area the size of an ECBilt

9   grid cell would have only partial coverage of permafrost.

10   Inaccuracy in model results is also expected since we cannot parameterize some of the snowpack

11   characteristics that alter the effect of snow on the ground thermal regime. Although we capture the role

12   of snow cover, which is to impose a reduced thermal diffusivity effect between the air and ground, there

13   are number of snowpack characteristics that we do not include such as rain-on-snow events and wind-

14   induced redistribution. As opposed to our generalized snowpack parameterization scheme, described in

15   section 2.1.1, high resolution snow models are fitted to observational data by analyzing, for example,

16   the physics of accumulation, areal distribution, and snow-soil interactions. Therefore, it is arguable from

17   this lack of details and the results shown in **Fig. 7**, whether the better option is to include a snowpack in

18   VAMPERS or not. However, we contend that the VAMPERS model is doing a reasonable job since it is

19   producing the surface offset that would naturally occur from the snowpack (Goodrich, 1982; Smith and

20   Riseborough, 2002). The simulated global distribution of this surface offset is shown in **Fig. 8**. It is

21   determined by calculating the difference between the mean annual ground temperature (MAGT) using

22   VAMPERS and the MAGT using VAMPER (no snow option and no imposed surface offset). Although the

23   maximum mean annual surface offset is about 12 °C, the average among all the grid cells that had snow

24   cover is about 2.7 C, which is close to our original applied surface offset of 2 °C in Kitover et al., (2013).

25   Values between 1 °C and 6 °C were reported early on by Gold and Lachenbruch (1973). Monitoring

26   studies of the air-ground temperature relationship also fall within this range e.g., Beltrami and Kellman

27   (2003), Bartlett et al., (2005), Grundstein et al., (2005), Zhang (2005). However, larger values of 10 °C

28   have been recorded in Alaska (Lawrence and Slater, 2010).

29   Further, without the snow option, changing precipitation patterns that can be the byproduct of a

30   shifting climate would otherwise have no effect on the subsurface thermal conditions. In other words,

31   the role of snow cover will be more noticeable in using the ECBilt-VAMPERS coupling when doing

32   transient experiments. An example of the effect of changing snow conditions on the ground thermal

33   regime come from Lawrence and Slater (2010), who demonstrated through experiments with the

34   Community Land Model that 1) increased snowfall accounted for 10 to 30% of soil warming and 2) a

35   shortened snow season also caused soil warming due to the ground surface's increased uncovered

36   exposure to air temperatures.   From this point forward, all analysis is done using results from VAMPERS

37   (i.e. *with* the snow option).

38   In addition to the surface offset imposed by incorporation of a snowpack, there are a number of factors

39   which have been commonly recognized in affecting the surface offset and hence should be part of the

40   air-ground coupling. Depending on the scale of interest, the magnitude of these can vary but they

1   include surface organic layer, vegetation, overlying water bodies, and wind. It should be recognized that
2   within ECBilt, some of these factors are reflected in the land surface temperature (notably wind and a
3   simplified vegetation scheme) but the others are absent. In addition, coupling the ECBilt surface
4   hydrology to the groundwater storage would affect both the ground thermal regime and hydrological
5   regime. In the first case, subsurface water content affects the thermal properties of the soil. In
6   particular, the conductivity of organics have high variation seasonally. In the second instance, frozen
7   ground is impermeable, allowing little or no subsurface water storage, in turn affecting runoff flow rates
8   and timing.

9   **3.2.2   Permafrost Thickness Validation**

10   The second validation examines the simulated depth of permafrost using borehole data taken from the
11   Global Terrestrial Network for Permafrost (GTN-P; www.gtnp.org). The scatterplot (**Fig. 9**) shows all the
12   observed borehole measurements mapped in **Fig. 10** versus the corresponding permafrost depth
13   simulated by *i*LOVECLIM. It is clear that there is a larger divergence between modeled and observed
14   depths for the deeper permafrost than for the more shallow observations, where the depths at some
15   points are overestimated by over 300 m and at some other points very underestimated by over 700 m.
16   There are a number of reasons to explain the mismatch, which can occur in the borehole data and/or
17   the model data. The first explanation is that the borehole estimates have a given range of uncertainty
18   since measurement techniques and subsequent interpretations are subject to error. Osterkamp and
19   Payne (1981) describe in detail potential errors associated with the freezing point depression, thermal
20   disturbance, and lithology.

21   The second cause is that we assumed implicitly that the observed permafrost depths are at equilibrium
22   with the current (or PI; preindustrial) climate state. This is probably why there is a mismatch at the
23   central Siberian site (66° 26' 2" N, 112° 26' 5" E) (point 1, **Fig. 9**), where the permafrost is estimated
24   from the borehole data to be 1000 m thick while the corresponding modeled value is only about 375 m.
25   It is very likely that, like much of the Siberian permafrost, this permafrost developed from the preceding
26   glacial period (Kondratjeva et al.,1993). Another example concerns western Siberia, (points 2 through 4,
27   **Fig. 9**), which is an area documented for having relict permafrost (Zemtsov and Shamakhov, 1992;
28   Ananjeva et al., 2003). It is also identified in the "Circumarctic Map of Permafrost and Ground-Ice
29   Conditions" (Brown et al., 2014) and "The Last Permafrost Maximum (LPM) map of the Northern
30   Hemisphere" (Vandenberghe et al., 2014). But it should be noted that not all the relict permafrost in
31   western Siberia is of late Pleistocene origin and may be from earlier cold stages (Zemtsov and
32   Shamakhov, 1992; French, 2007).

33   Another reason for some discrepancies between modeled and observed data is that high-resolution
34   features in the landscape and topography cannot be captured by *i*LOVECLIM due to the limited spatial
35   resolution and hence, a small set of model parameters. Such factors as vegetation and organic layer,
36   which can vary due to local topography and micro-climatic conditions, have been shown to affect the
37   active layer and ground thermal regime (Shur and Yorgenson, 2007; Fukui et al., 2008; Lewkowicz et al.,
38   2011; Wang et al., 2014). Consequently, given a specific borehole site, some discrepancy in the
39   permafrost thickness estimate will likely occur between our simplified interpretation and that which

1 results from including more complex and local interactions. It is possible, for example, that the observed
2 value for point 5 (720 m) is a function of higher elevation since it is from a borehole site in the Russia
3 Highlands but this relatively local elevation effect may not be a strong enough signal in the *i*LOVECLIM
4 surface temperatures, and hence is underestimated.

5 The other outlying points (points 6 and 7, **Fig. 9**) occur in Canada but as opposed to the relict sites as
6 mentioned above, *i*LOVECLIM overestimates the permafrost thickness.. These discrepancies, both
7 occurring at high latitudes of 80 °N and 76 °N , reveal that VAMPERS is not reproducing the subsurface
8 temperatures well for this area. For example, a report for the specific borehole (Gemini E-10; point 6,
9 **Fig. 9**) calculated the geothermal gradient to be approximately 0.04 °C/m (Kutasov and Eppelbaum,
10 2009) whereas our model result for the corresponding grid space found a gradient of approximately 0.03
11 °C/m. Although this difference is relatively small, it hints at either a necessary increase in the averaged
12 geothermal heat flux used in the model or a change in the subsurface thermal properties (increase in
13 thermal conductivity), which could be altered by an adjustment in the VAMPERS water content.
14
15 **3.2.3   Climate analysis**

16 Finally, the remaining possibility to explain inaccuracies between the modeled results and the observed
17 results (both in reproducing spatial extent and permafrost thickness) is the *i*LOVECLIM climate. Results
18 of the VAMPER(S) model, above all other parameter settings, are most dependent on the mean annual
19 ground surface temperature, as shown in the sensitivity study from Kitover et al. (2013), so if there
20 exists biases or discrepancies within the forcing, it will be reflected in the output. For this portion of our
21 analysis, we took observed mean annual ground temperature (MAGT) measurements from again the
22 GTN-P (IPY Thermal State of Permafrost Snapshot, IPA 2010) . As a result, we composed a 1:1
23 comparison between the observed MAGT and the corresponding simulated MAGT at the same
24 approximate depth and location (**Fig. 11**). **Figure 12** shows a map of the selected GTN-P measurements.
25 All the temperature comparisons are within the top thirty meters of the subsurface and therefore reflect
26 the present or very recent climate as opposed to the deeper temperatures (i.e., > 150 m) that,
27 depending on subsurface thermal diffusivity and surface temperature perturbations, can reflect
28 historical temperatures of at least one hundred years ago (Huang et al., 2000) and up to tens of
29 thousands of years (Ter Voorde et al., 2014).

30 **Fig. 11** illustrates that VAMPERS does a reasonable job of predicting shallow subsurface temperatures
31 since the Pearson correlation is about 0.64. This result, therefore, supports the notion that the
32 preindustrial climate is well represented by *i*LOVECLIM. The points of Kazakhstan and Mongolia, and a
33 few others in Russia, have a warm bias in the forcing (simulated is warmer than observed), which is
34 probably due to an inaccurate representation of elevation temperature changes in *i*LOVECLIM, since
35 many of those sites are at elevations above 1000 m. Even applying the lapse rate for a standard profile
36 (6.5 C / km; McGuffie & Henderson-Sellers, 2013) would presumably make a significant difference on
37 the depth since earlier sensitivity tests (Kitover et al., 2013) showed an average 55 m increase in
38 equilibrium permafrost depth for every 1 °C colder. On the other hand, many of the other points show
39 that predicted subsurface temperatures are on average a few degrees colder than the observed, leading
40 to the most obvious conclusion that a cold bias exists in the *i*LOVECLIM climate. Although the cold bias,

1 most obvious for Canada and Alaska, is congruent to the overestimation in permafrost thickness evident
2 from the geographic breakdown illustrated in **Fig. 10**, it has not previously been substantiated in former
3 analyses of LOVECLIM or *i*LOVECLIM so it is more likely that such a discrepancy is due to the air-ground
4 coupling as opposed to simply the land surface temperature forcing. Indeed, there a number of other
5 (sub)surface processes not included in the current ECBilt-VAMPERS coupling which may reduce the
6 apparent cold bias. These effects alter the seasonal behavior of the thermal diffusivity in the subsurface
7 and have been well-documented in observational studies (Williams and Burn, 1996; Woo and Xia, 1996;
8 Fukui et al., 2008). Smith and Riseborough (2002) simplified these mechanisms into the surface offset
9 (air to ground surface) and the thermal offset (ground surface to top of the permafrost). Due to minimal
10 complexity of the VAMPERS model, these offsets may be somewhat overlooked.

11 For now, the average range of error between observed and predicted is about 2.6 °C. Given that the
12 comparisons are between point-based observations and large grid cell values, meant to represent a
13 relatively large surface area, some variability is expected to occur.

14 **4   Future Development**

15 The results of this paper demonstrate the ability of VAMPERS forced by *i*LOVECLIM to model current
16 permafrost distribution and thickness. The next step is to analyze the feedback that permafrost changes
17 have on the climate. This has been of particular interest of the last decade since it is clear that specific
18 feedbacks exists, most notably the release of locked-up carbon in the atmosphere as permafrost
19 degrades (Anisimov, 2007). The initial method behind a full coupling would be to activate the coupling
20 mechanisms, shown in **Fig. 3,** and reanalyze the equilibrium results (since a full coupling would likely
21 lead to an altered equilibrium permafrost state). In addition, the feedback effects would be most visible
22 during millennial-scale transient climate shifts, when major permafrost degradation and/or
23 disappearance is likely to occur.

24 **5   Conclusions**

25 Enhancements have been made to the VAMPER model to make possible an estimated present-day
26 distribution of permafrost thickness and distribution using ECBilt land surface temperatures within the
27 *i*LOVECLIM equilibriated preindustrial climate as the forcing. The change in timestep to 4 hours was
28 necessary to match the timestep of ECBilt and allow the seasonal effects, notably snow cover and the
29 active layer, to be reflected in the simulation of permafrost. The predicted annual active layer from the
30 stand-alone VAMPER model, under different temperature forcings, compare well with results from the
31 Stefan equation. We also described the snow option, which introduces the thermal insulation effects
32 and changes in the thermal properties of snow over time due to varying snow densities. In addition, we
33 developed two new maps: geothermal heat flux and porosity. Incorporating these parameters at a
34 global scale was an important step in improving the horizontal spatial variability of permafrost
35 thickness/distribution while also maintaining the simplicity and efficiency of ECBilt-VAMPERS.

36   Equilibrium experiments for the PI climate show that when the snow component is included in the
37 VAMPER model, the permafrost extent is noticeably reduced while the average surface offset of 2.7 °C is
38 comparable to previous reports. We then compared both permafrost thickness estimates and

1   subsurface temperatures to corresponding observed values. Considering that we are comparing point

2   measurements to gridcell-based values, the simulations are reasonable. There are some discussion

3   points around the discrepancies. One is that the relatively coarse horizontal ECBilt grid will never

4   perfectly match the sensitivity of permafrost occurrence and depth due to local factors. This is also the

5   case in the air-land temperature coupling, where some of the local effects will simply not be present in

6   an EMIC. Similarly, when *i*LOVECLIM does not accurately represent the environmental lapse rate in areas

7   of higher elevation, the occurrence of permafrost in these areas are overlooked by the VAMPERS model.

8   Finally, some of the observed permafrost depths are not a function of the present (PI) climate, but

9   rather a relict presence from previous cold periods. Therefore, when comparing measured to simulated

10   results, some underestimations occurred. It is only with millennial-scale transient *i*LOVECLIM (with the

11   ECBilt-VAMPERS coupling) model runs that we can simulate, for example in areas of West Siberia, how

12   permafrost evolved over periods of major climate change.

13

14   **6   Code availability**

15   The *i*LOVECLIM (version 1.0) source code is based on the LOVECLIM model version 1.2 whose code is

16   accessible at http://www.elic.ucl.ac.be/modx/elic/index.php?id=289. The developments on the

17   *i*LOVECLIM and VAMPER(S) source code are hosted at https://forge.ipsl.jussieu.fr/ludus but are not

18   publicly available due copyright restrictions. Access can be granted on demand by request to D. M.

19   Roche (didier.roche@lsce.ipsl.fr).

1 **References**

2

3 Almén, K., Andersson, J. , Carlsson, L., Hansson, K., and Larsson, N.: Hydraulic testing in crystalline rock.
4 A comparative study of single-hole test methods, Swedish Nuclear Fuel and Management Company,
5 Uppsala, Sweden, SKB Technical Report 86-27, 190 pp., 1986.

6 Ananjeva (Malkova), G.V., Melnikov, E.S., and Ponomareva, O.E.: Relict permafrost in the central part of
7 western Siberia, in: Proceedings of 8th International Conference on Permafrost, Zurich, Switzerland, 5-8,
8 2003.

9 Anisimov, O.A.: Potential feedback of thawing permafrost to the global climate system through methane
10 emission, Environ. Res. Lett., 2, 045016, doi:10.1088/1748-9326/2/4/045016, 2007.

11 Anisimov, O.A. and Nelson, F.E.: Permafrost distribution in the Northern Hemisphere under scenarios of
12 climatic change, Global and Planetary Change, 14, 59-72, 1996.

13 Athy, L.F.: Density, porosity, and compaction of sedimentary rocks, Am. Assoc. Petrol. Geol. Bull, 14, 1-
14 24, 1930.

15 Avis, C.A., Weaver, A.J., and Meissner, K.J.: Reduction in areal extent of high-latitude wetlands in
16 response to permafrost thaw, Nature Geosci, 4, 444-448, 2011.

17 Bartlett, M.G., Chapman, D.S., and Harris, R.N.: Snow effect on North American ground temperature
18 1950-2002, J. Geophy. Res., 110, F03008, doi: 10.1029/2005JF000293, 2005.

19 Beltrami, H. and Kellman, L.: An examination of short- and long-term air–ground temperature coupling,
20 Global Planet. Change, 38, 291-303, 2003.

21 Burn, C.R and Nelson, F.E.: Comment on ''A projection of severe near-surface permafrost degradation
22 during the 21st century'' by David M. Lawrence and Andrew G. Slater, Geophy. Res. Lett., 33, L21503,
23 doi:10.1029/2006GL027077, 2006.

24 Buteau, S., Fortier, R., Delisle, G., and Allard, M.: Numerical simulation of the impacts of climate
25 warming on a permafrost mound, Permafrost Periglac., 15, 41-57, 2004.

26 Brouchkov, A., Fukuda, M., Iwahana, G., Kobayashi, Y., and Konstantinov, P.: Thermal conductivity of
27 soils in the active layer of eastern Siberia, Permafrost Periglac., 16, 217-222, 2005.

28 Brown, J., Ferrians, O., Heginbottom, J.A., and Melnikov, E.: Circum-Arctic Map of Permafrost and
29 Ground-Ice Conditions, National Snow and Ice Data Center, Boulder, CO, 2014.

30 Cheng, G. and Wu, T.: Responses of permafrost to climate change and their environmental significance,
31 Qinghai-Tibet Plateau, J. Geophy. Res., 112, F02S03, doi:10.1029/2006JF000631, 2007.

32 Claussen, M., Mysak, L.A., Weaver, A.J, Crucifix, M., Fichefet, T., Loutre, M.-F., Weber, S.L., Alcamo, J.,
33 Alexeev, V.A., Berger, A., Calov, R., Ganopolski, A., Goosse, H., Lohmann, G., Lunkeit, F., Mokhov, I.I.,

18

1 Petoukhov, V., Stone, P., and Wang, Z.: Earth system models of intermediate complexity: closing the gap
2 in the spectrum of climate system models, Clim. Dynam., 18, 579-186, 2002.

3 Dankers, R., Burke, E.J. and Price J.: Simulation of permafrost and seasonal thaw depth in the JULES land
4 surface scheme, The Cryosphere, 5, 773-790, 2011.

5 Davidson, E.A. and Janssens, I.A.: Temperature sensitivity of soil carbon decomposition and feedbacks to
6 climate change, Nature, 440, 165-173, doi:10.1038/nature04514, 2006.

7 Davies, J.H.: Global map of solid earth heat flow, Geochem. Geophy. Geosy., 14, 4608-4622, doi:
8 10.1002/ggge.20271, 2013.

9 DeConto, R.M., Galeotti, S., Pagani, M., Tracy, D., Schaefer, K., Zhang, T., Pollard, D. and Beerling, D.J.:
10 Past extreme warming events linked to massive carbon release from thawing permafrost, Nature,   484,
11 87 – 91, doi:10.1038/nature10929, 2012.Delisle, G.: Numerical simulation of permafrost growth and
12 decay, J. Quaternary Sci., 13, 325-333, 1998.

13 Dingman, S.L.: Physical Hydrology, Second Edition, Prentice Hall, Upper Saddle River, N.J., 2002.

14 Ekici, A., Beer, C., Hagemann, S., Boike, J., Langer, M., and Hauck, C.: Simulating high-latitude permafrost
15 regions by the JSBACH terrestrial ecosystem model, Geosci. Model Dev., 7, 631-647, doi: 10.5194/gmd-
16 7-631-2014 2014.

17 Farouki, O.T.: Thermal properties of soils, Cold Regions Research and Engineering Laboratory, Hannover,
18 N.H., CRREL Report 81-1, 136 pp., 1981.

19 Fox, J.D.: Incorporating freeze-thaw calculations into a water balance model, Water Resour. Res., 38,
20 2229-2244, 1992.

21 French, H.M.: The Periglacial Environment, Third Edition, Jon Wiley & Sons Ltd, West Sussex, England,
22 2007.

23 Fukui, K., Sone, T., Yamagata, K., Otsuki, Y., Sawada, Y., Vetrova, V., and Vyatkina, M.: Relationships
24 between permafrost distribution and surface organic layers near Esso, Central Kamchatka, Russian Far
25 East, Permafrost Periglac., 19, 85-92, doi: 10.1002/ppp.606, 2008.

26 Genxu, W., Hongchang H., and Taibin L.: The influence of freeze–thaw cycles of active soil layer on
27 surface runoff in a permafrost watershed, J. Hydrol., 375, 438-449, doi: 10.1016/j.jhydrol.2009.06.046,
28 2009.

29 Gleeson, T., Moosdorf, N., Hartmann, J., and van Beek, L. P. H.: A glimpse beneath earth's surface:
30 GLobal HYdrogeology MaPS (GLHYMPS) of permeability and porosity, Geophys. Res. Lett., 41,
31 2014GL059856, doi:10.1002/2014gl059856, 2014.

1 Gold, L.W. and Lachenbruch, A.H.: Thermal conditions in permafrost - a review of North American
2 literature, in: Permafrost: The North American Contribution to the Second International Conference,
3 Yakustsk, USSR, 13-28 July 1973, 3-23, 1973.

4 Goodrich, L.E.: The influence of snow cover on the ground thermal regime, Can. Geotech. J., 19, 421-
5 432, 1982.

6 Goosse, H. and Fichefet, T.: Importance of ice-ocean interactions for the global ocean circulation: A
7 model study, J. Geophys. Res., 104, 23337–23355, doi: 10.1029/1999JC900215, 1999.

8 Goosse, H., Renssen, H., Timmermann, A., and Bradley, R. S.: Internal and forced climate variability
9 during the last millennium: a model-data comparison using ensemble simulations, Quaternary Sci. Rev.,
10 24, 1345–1360, 2005.

11 Goosse, H., Brovkin, V., Fichefet, T., Haarsma, R., Huybrechts, P., Jongma, J., Mouchet, A., Selten, F.,
12 Barriat, P.Y., Campin, J., Deleersnijder, E., Driesschaert, E., Goelzer, H., Janssens, I., Loutre, M., Morales
13 Maqueda, M.A., Opsteegh, T., Mathieu, P., Munhoven, G., Pettersson, E.J., Renssen, H., Roche, D.M.,
14 Schaeffer, M., Tartinville, B., Timmermann, A., and Weber, S.L: Description of the earth system model of
15 intermediate complexity LOVECLIM version 1.2, Geosci. Model Dev., 3, 603-633, DOI: 10.5194/gmd-3-
16 603-2010, 2010.

17 Grundstein, A., Todhunter, P., and Mote, T.: Snowpack control over the thermal offset of air and soil
18 temperatures in eastern North Dakota, Geophy. Res. Lett., 32, L08503, doi:10.1029/2005GL022532,
19 2005.

20 Hartmann, J. and Moosdorf, N.: The new global lithological map database GLiM: A representation of
21 rock properties at the Earth surface, Geochem. Geophy. Geosy., 13, Q12004,
22 doi:10.1029/2012GC004370, 2012.

23 Hinzman, L.D. and Kane, D.L.: Potential Repsonse of an Arctic Watershed During a Period of Global
24 Warming, J. Geophys. Res., 97, 2811-2820, 1992.

25 Huang, S., Pollack, H.N., and Shen, P.: Temperature trends over the past five centuries reconstructed
26 from borehole temperatures, Nature, 403, 756-758, 2000.

27 Kitover, D.C., Renssen, H., Vandenberghe, J., and van Balen, R.T.: Modeling permafrost response of the
28 last glacial termination: first results of the VAMPER model, in: Proceedings of the 10th International
29 Conference on Permafrost, Salekhard, Russia, 25-29 June 2012, 209-214, 2012.

30 Kitover, D.C., van Balen, R.T., Roche, D.M., Vandenberghe, J., and Renssen, H.: New estimates of
31 permafrost evolution during the last 21 k years in Eurasia using numerical modelling, Permafrost
32 Periglac., 24, 286-303, 2013.

1   Kondratjeva, K.A., Khrutzky, S.F., and Romanovsky, N.N.: Changes in the extent of permafrost during the
2   late Quaternary period in the territory of the former Soviet Union, Permafrost Periglac., 4, 113-119,
3   1993.

4   Koven, C.D., Ringeval, B. Friedlingstein, P., Ciais, P., Khvorostyanov, D., Krinner, G., and Tarnocai C.:
5   Permafrost carbon-climate feedbacks accelerate global warming, Proc. Natl. Acad. Sci. USA, 108, doi:
6   10.1073/pnas.1103910108, 2011.

7   Koven, C.D., Riley, W.J., and Stern, A.: Analysis of permafrost thermal dynamics and response to climate
8   change in the CMIP5 earth system models, J. Climate, 26, 1877-1900, doi: 10.1175/JCLI-D-12-00228.1,
9   2013.

10   Kutasov, I.M. and Eppelbaum, L.V.: Estimation of geothermal gradients from single temperature log-field
11   cases, J. Geophys. Eng., 6, 131-135, doi: 10.1088/1742-2132/6/2/004, 2009.

12   Lawrence, D.M. and Slater, A.G.: A projection of severe near-surface permafrost degradation during the
13   21st century, Geophy. Res. Lett. , 32, L24401, doi: 10.1029/2005GL025080, 2005.

14   Lawrence, D.M. and Slater, A.G:. The contribution of snow condition trends to future ground climate,
15   Clim. Dyn., 34, 969-981, doi: 10.1007/s00382-009-0537-4, 2010.

16   Lawrence, D.M., Oleson, K.W., Flanner, M.G., Thornton, P.E., Swenson, S.C., Lawrence, P.J., Zeng, X.,
17   Yang, Z., Levis, S., Sakaguchi, K., Bonan, G.B., and Slater, A.G.: Parameterization improvements and
18   functional and structural advances in Version 4 of the Community Land Model, J. Adv. Model. Earth
19   Syst., 3, M03001, doi: 10.1029/2011MS000045, 2011.

20   Lebret, P., Dupas, A., Clet, M., Coutard, J., Lautridou, J., Courbouleix, S., Garcin, M., Levy, M., and Van
21   Vliet-Lanoë, B.: Modelling of permafrost thickness during the late glacial stage in France: preliminary
22   results, Can. J. Earth Sci., 31, 959-968, 1994.

23   Lewkowicz, A.G., Etzelmuller, B., and Smith, S.: Characteristics of discontinuous permafrost based on
24   ground temperature measurements and electrical resistivity tomography, Southern Yukon, Canada,
25   Permafrost Periglac., 22, 320-342, doi: 10.1002/ppp.703, 2011.

26   Li, X. and Koike, T.: Frozen soil parameterization in SiB2 and its validation with GAME-Tibet observations,
27   Cold Reg. Sci. Technol, 36, 165-182, doi: 10.1016/S0165-232X(03)00009-0, 2003.

28   Ling, F. and Zhang, T.: A numerical model for surface energy balance and thermal regime of the active
29   layer and permafrost containing unfrozen water, Cold Reg. Sci. Technol., 38, 1-15, 2004.

30   Lunardini, V.J. Permafrost formation time, Cold Regions Research and Engineering Laboratory,
31   Hannover, N.H., CRREL Report 95-8, 1995.

32   Lynch-Stieglitz, M.: The development and validation of a simple snow model for the GISS GCM, J.
33   Climate, 7, 1842–1855, 1994.

1 McGuffie, K. and Henderson-Sellers, A.: A Climate Modelling Primer, John Wiley & Sons, Ltd., West
2 Sussex, England, 2013.

3 Mottaghy, D. and Rath, V.: Latent heat effects in subsurface heat transport modelling and their impact
4 on palaeotemperature reconstructions, Geophys. J. Int., 164, 236–245, doi: 10.1111/j.1365-
5 246X.2005.02843.x, 2006.

6 Nicolsky, N.J., Romanovsky, V.E., and Panteleev, G.G.: Estimation of soil thermal properties using in-situ
7 temperature measurements in the active layer and permafrost, , Cold Reg. Sci. Technol, 55, 120-129,
8 2009.
9
10 Nováková, L., Sosna, K., Brož, M., Najser, J ., and Novák, P.: The matrix porosity and related properties
11 of a leucocratic granite from the Krudum Massif, West Bohemia, Acta Geodyn. Geomater., 9, 521-540,
12 2012.

13 Opsteegh, J., Haarsma, R., Selten, F., and Kattenberg, A.: ECBILT: A dynamic alternative to mixed
14 boundary conditions in ocean models, Tellus, 50, 348–367, 1998.

15 Osterkamp, T.E. and Gosink, J.P.: Variations in permafrost thickness in response to changes in
16 paleoclimate, J. Geophys. Res., 96, 4423-4434, 1991.

17 Osterkamp, T.E. and Payne, M.W.: Estimates of permafrost thickness from well logs in northern Alaska,
18 Cold Reg. Sci. Technol, 5, 13-27, 1981.

19 Pitman, A.J., Yang, Z-L., Cogley, J.G., and Henderson-Sellers, A.: Description of bare essentials of surface
20 transfer for the Bureau of Meteorological Research Centre AGCM, BRMC, Australia, BMRC Research
21 Report 32, 117 pp., 1991.

22 Renssen, H., Goosse, H., Fichefet, T., Brovkin, V., Driesschaert, E., and Wolk, F.: Simulating the Holocene
23 climate evolution at northern high latitudes using a coupled atmosphere-sea ice-ocean-vegetation
24 model, Clim. Dynam., 24, 23–43, doi: 10.1007/s00382-004-0485-y, 2005.

25 Renssen, H., Seppä, H., Heiri, O., Roche, D. M., Goosse, H., and Fichefet, T.: The spatial and temporal
26 complexity of the Holocene thermal maximum, Nat. Geosci., 2, 411–414, doi: 10.1038/ngeo513, 2009.

27 Roche, D.M.: δ^{18}O water isotope in the *i*LOVECLIM model (version 1.0) – Part 1: Implementation and
28 verification, Geosci. Model Dev., 6, 1481-1491, doi:10.5194/gmd-6-1481-2013, 2013.

29 Roche, D.M., Dokken, T.M., Goosse, H., Renssen, H., and Weber, S.L.: Climate of the last glacial
30 maximum: sensitivity studies and model-data comparison with the LOVECLIM coupled model, Clim. Past,
31 3, 205-224, 2007.

32 Roche, D.M., Dumas, C., Bügelmayer, M., Charbit, S., and Ritz, C.: Adding a dynamical cryosphere to
33 *i*LOVECLIM (version 1.0): coupling with the GRISLI ice-sheet model, Geosci. Model Dev., 7, 1377-1394,
34 doi: 10.5194/gmd-7-1377-2014, 2014.

1 Roche, D.M., Renssen, H., Paillard, D., and Levavasseur, G.: Deciphering the spatio-temporal complexity
2 of climate change of the last deglaciation: a model analysis, Clim. Past, 7, 591-602, doi: 10.5194/cp-3-
3 205-2007, 2011.

4 Romanovsky, V.E. and Osterkamp, T.E.: Interannual variations of the thermal regime of the active layer
5 and near-surface permafrost in northern Alaska, Permafrost Periglac., 6, 313-335, 1995.

6 Schaefer, K., Zhang, T., Bruhwiler, L. and Barret, A.P.: Amount and timing of permafrost carbon release in
7 response to climate warming, Tellus Series B Chemical and Physical Meteorology , 63B, 165-180, 2011.

8 Schild, M., Siegesmund, S., Vollbrecht, A., and Mazurek, M.: Characterization of granite matrix porosity
9 and pore-space geometry by in situ and laboratory methods, Geophys. J. Int., 146, 111-125, 2001.

10 Schneider von Deimling, T., Meinshausen, M., Levermann, M., Huber, V., Frieler, K., Lawrence, D.M.,
11 and Brovkin, V.: Estimating the near-surface permafrost-carbon feedback on global warming,
12 Biogeosciences, 9, 649-665, 2012.

13 Shur, Y.L. and Jorgenson, M.T.: Patterns of permafrost formation and degradation in relation to climate
14 and ecosystems, Permafrost Periglac., 18, 7-19, doi: 10.1002/ppp.582, 2007.

15 Smith, M.W. and Riseborough, D.W.: Climate and the limits of permafrost: A zonal analysis, Permafrost
16 Periglac., 13, 1-15, 2002.

17 Stendel, M. and Christensen, J.H.: Impact of global warming on permafrost conditions in a coupled GCM,
18 Geophy. Res. Lett., 29, doi: 10.1029/2001GL014345, 2002.

19 Ter Voorde, M., van Balen, R., Luijendijk, E., and Kooi, H.: Weichselian and Holocene climate history
20 reflected in temperatures in the upper crust of the Netherlands, Neth. J. Geosci., 93, 107-117,
21 doi:10.1017/njg.2014.9, 2014.

22 Vandenberghe, J., French, H.M., Gorbunov, A., Marchenko, S., Velichko, A.A., Jin, H., Cui, Z., Zhang, T.,
23 and Wan, X.: The Last Permafrost Maximum (LPM) map of the Northern Hemisphere: permafrost extent
24 and mean annual temperatures, 25-17 ka BP, Boreas, 43, 652-666, doi: 10.1111/bor.12070, 2014.

25 Verseghy, D.L.: CLASS-A Canadian land surface scheme for GCMS I. Soil model, Int. J. Climatol., 11, 111-
26 133, 1991.

27 Wang, G., Mao, T., Chang, J., and Du, J.: Impacts of surface soil organic content on the soil thermal
28 dynamics of alpine meadows in permafrost regions: data from field observations, Geoderma, 232-234,
29 414-425, doi: 10.1016/j.geoderma.2014.05.016, 2014.

30 Weber, S.L.: The utility of Earth system Models of Intermediate Complexity (EMICs), WIREs Climate
31 Change, 1, 243-252, doi: 10.1002/wcc.24, 2010.

32 Williams, D.J. and Burn, C.R.: Surficial characteristics associated with the occurrence of permafrost near
33 Mayo, Central Yukon Terrritory, Canada, Permafrost Periglac., 7, 193-206, 1996.

1   Williams, P.J. and Smith, M.W.: The Frozen Earth: Fundamentals of Geocryology, Cambridge University
2   Press, Cambridge, England, 2007.

3   Woo, M.K. and Xia, Z.: Effects of hydrology on the thermal conditions of the active layer, Nordic
4   Hydrology, 27, 129–142, 1996.

5   Zemtsov, A.A. and Shamakhov. A.F.: Characteristics of relict permafrost on the west Siberian plain, Polar
6   Geography and Geology, 17, 245-250, 1993.

7   Zhang, T.: Influence of the seasonal snow cover on the ground thermal regime: an overview, Rev.
8   Geophys., 43, RG4002, doi:10.1029/2004RG000157, 2005.

9   Zhang, Y., Carey, S.K., and Quinton, W.L.: Evaluation of the algorithms and parameterizations for ground
10 thawing and freezing simulation in permafrost regions. J. Geophys. Res., 113, D17116, DOI:
11 10.1029/2007JD009343, 2008.

12 Zhang, Y., Chen, W., and Riseborough, D.: Temporal and spatial changes of permafrost in Canada since
13 the end of the Little Ice Age. J. Geophys. Res., 111, doi:10.1029/2006JD007284, 2006.

14

1   Table 1. Variable values applied in the Stefan equation.

Variables		
thermal conductivity (k_{mw})	1.7	W m^{-1} K^{-1}
dry density of soil (ρ_m)	1600	kg m^{-3}
latent heat of fusion (L)	334	kJ kg^{-1}
total moisture content (W)	0.3	-
unfrozen water conent (W_u)	0	-

2
3

1 Table 2. Calculated maximum annual active layer thickness using both the Stefan Equation and the
2 VAMPER model under different forcing scenarios.

Model Run	Average Annual Ground Surface Temperature	Annual Amplitude	Stefan Equation Active Layer	Vamper Model Active Layer
	(°C)	(°C)	(m)	(m)
1	-6	10	0.7	0.7
2	-4	10	1.0	1.0
3	-2	10	1.2	1.3
5	-6	20	1.6	1.7
6	-4	20	1.7	1.9
7	-2	20	1.9	1.9

3
4
5
6

1   Table 3. The original lithological classification from Hartmann and Moosdorf (2012) and the
2   reclassification scheme used for the ECBilt grid.
3

	Original Litho Class	VAMPER Class
1	Unconsolidated Sediments (SU)	Sed
2	Basic Volcanic Rocks (VB)	Bed
3	Siliciclastic Sedimentary Rocks (SS)	Sed
4	Basic Plutonic Rocks (PB)	Bed
5	Mixed Sedimentary Rocks (SM)	Sed
6	Carbonate Sedimentary Rocks (SC)	Sed
7	Acid Volcanic Rocks (VA)	Bed
8	Metamorphic Rocks (MT)	Bed
9	Acid Plutonic Rocks (PA)	Bed
10	Intermediate Volcanic Rocks (VI)	Bed
11	Water Bodies (WB)	N/A
13	Pyroclastics (PY)	Bed
12	Intermediate Plutonic Rocks (PI)	Bed
15	Evaporites (EV)	Sed
14	No Data (ND)	N/A
16	Ice and Glaciers (IG)	N/A
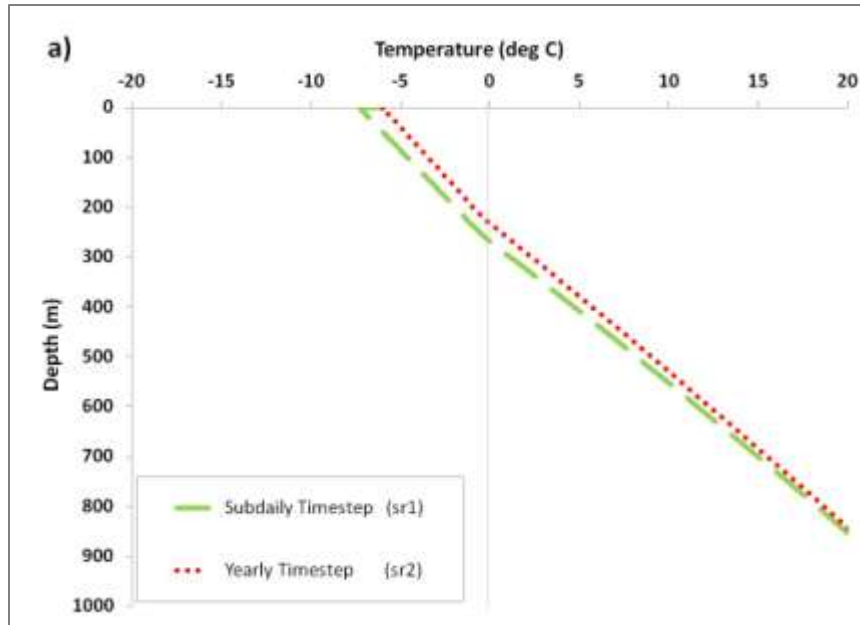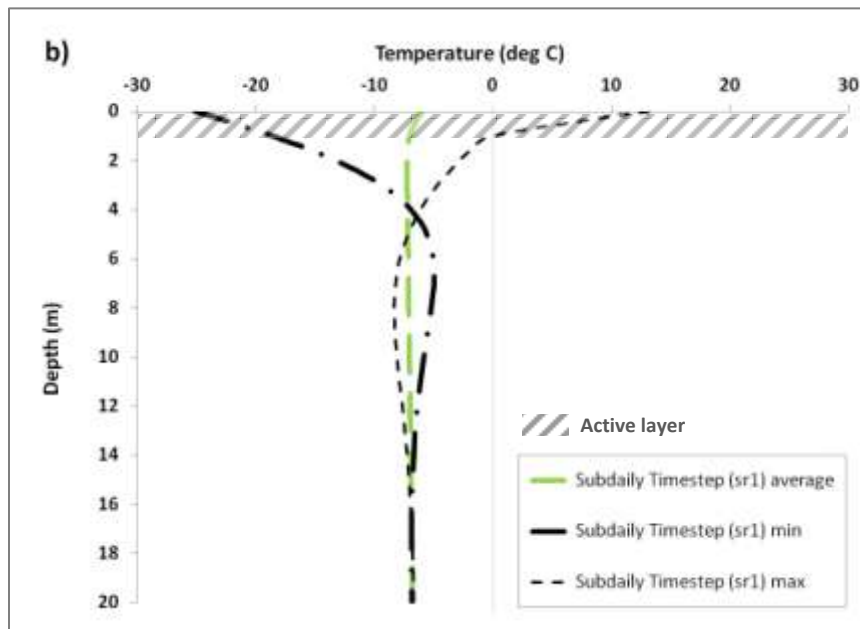
4

Figure 1. a) Plot comparing VAMPER model results using different timesteps (annual vs. subdaily) but the same annual average temperature forcing of -6 °C. b) Plot showing the sr1 average, min, and max temperature-depth profiles. Also shown in b) is the ~ 1 m active layer, marked as diagonal lines.
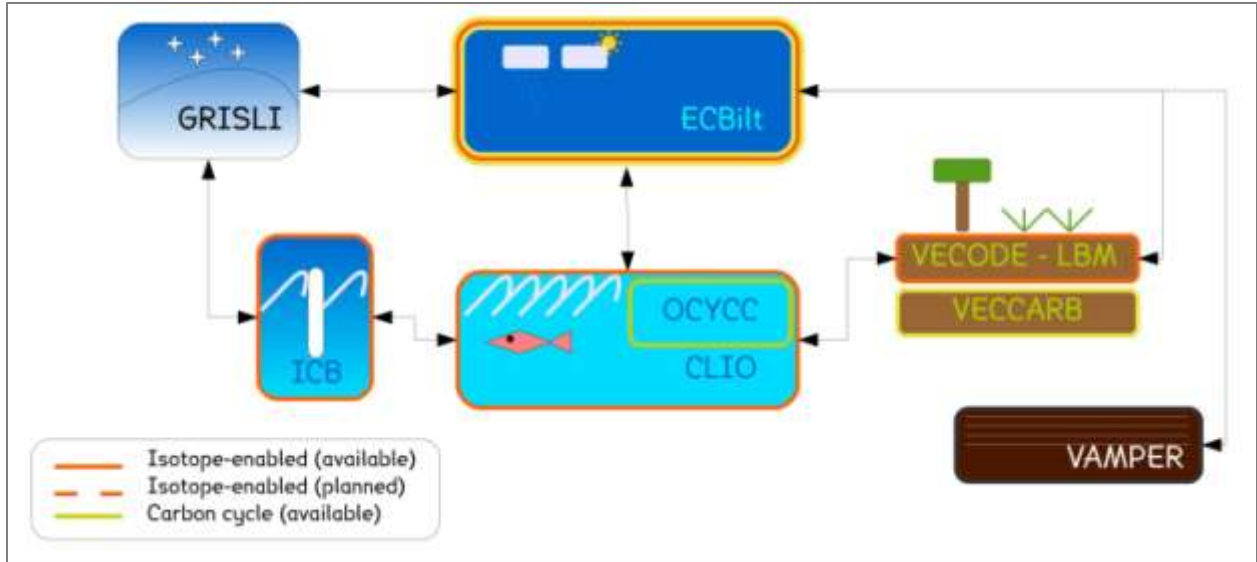
Figure 2. *i*LOVECLIM model component setup.

1
2
3
4
5
6
7
8
9
10
11
12
13
14
15
16
17
18
19
20
21
22
23
24
25
26
27
28
29
30
31
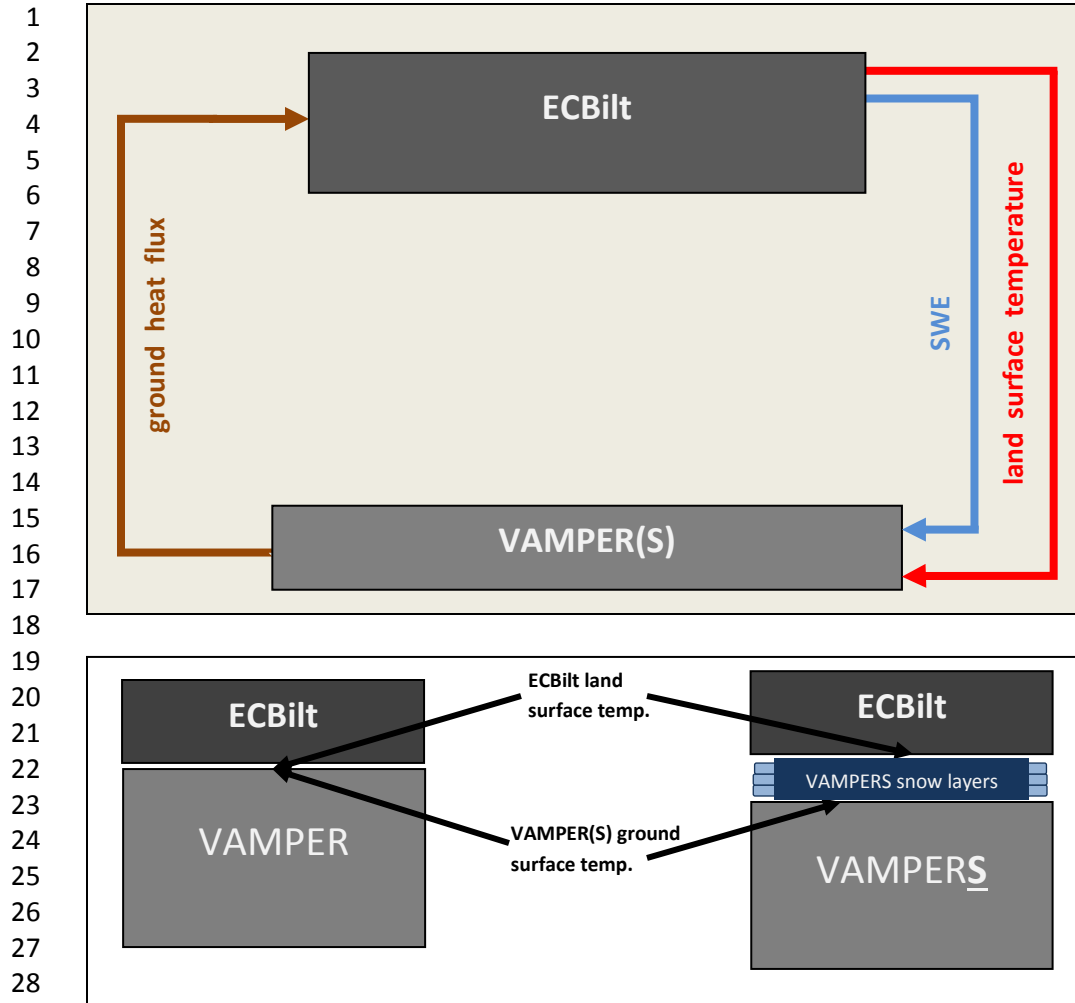
Figure 3 a). Future *i*LOVECLIM coupling scheme between ECBilt and the VAMPER(S) model showing the variables (land surface temperature, snow water equivalent (swe), and ground heat flux) passed between the components at each timestep. b) Land surface temperature of ECBilt and ground surface temperature of VAMPER(S).
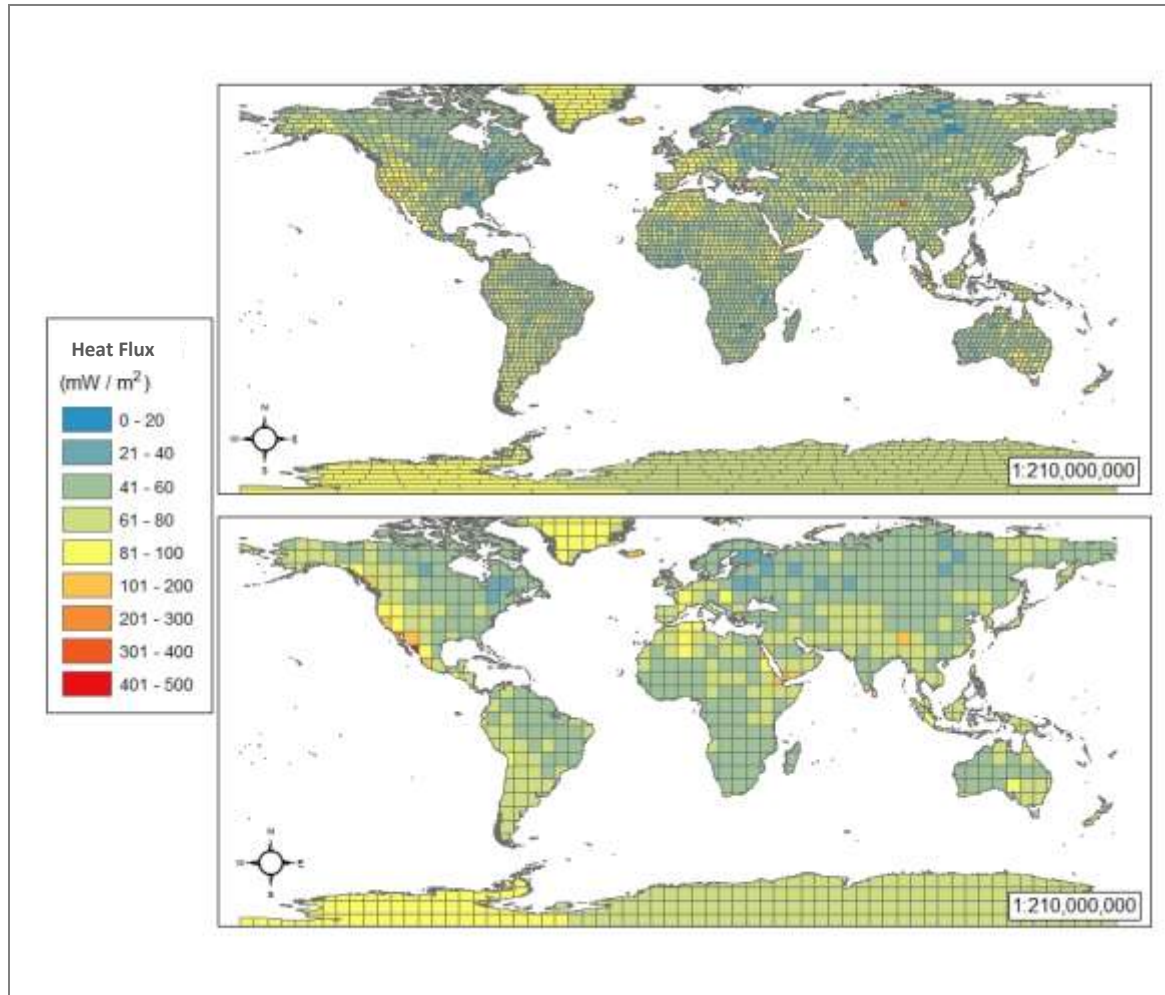
Figure 4. The original geothermal heat flux map (top) from Davies (2013) and the weighted average version (top) for use as the lower boundary value in the *i*LOVECLIM experiments (bottom).
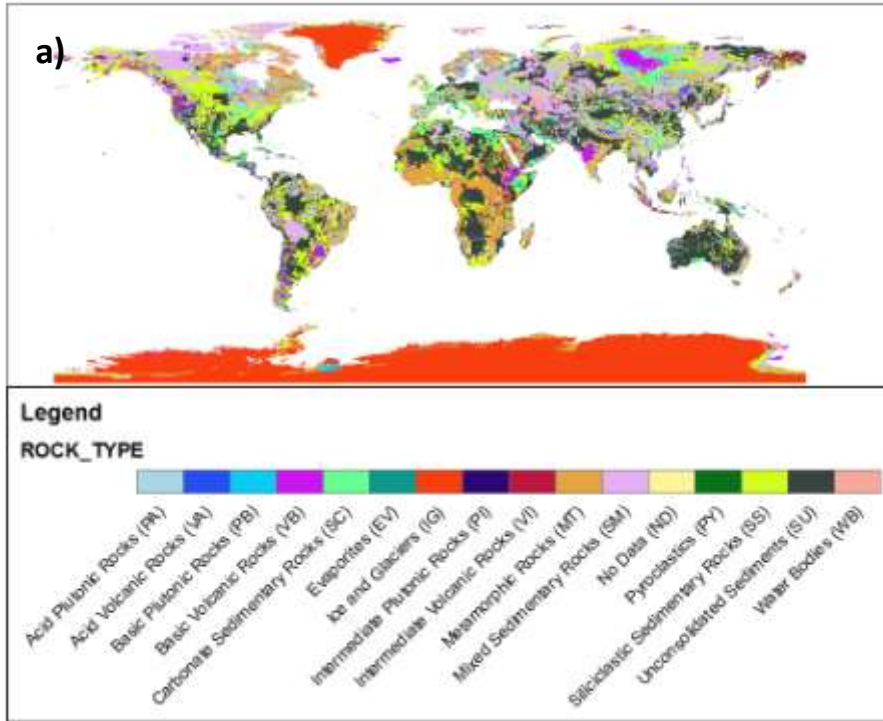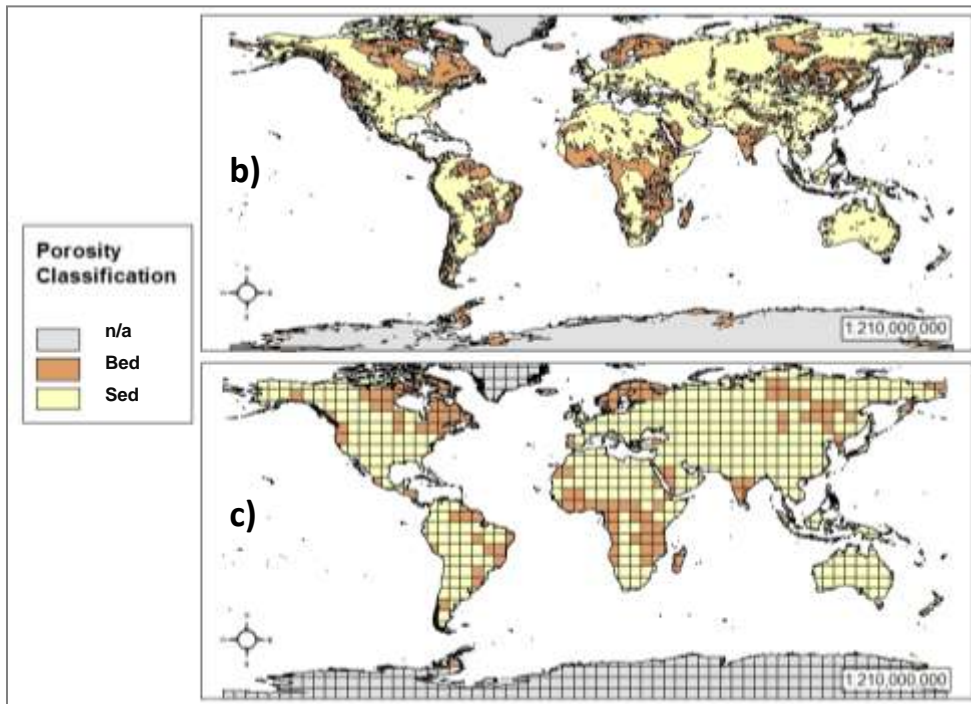
Figure 5. World maps showing a) original map from Hartmann and Moosdorf (2012) b) map of reclassified lithology using Table 2 and c) the version geo-processed to match the ECBilt grid resolution.
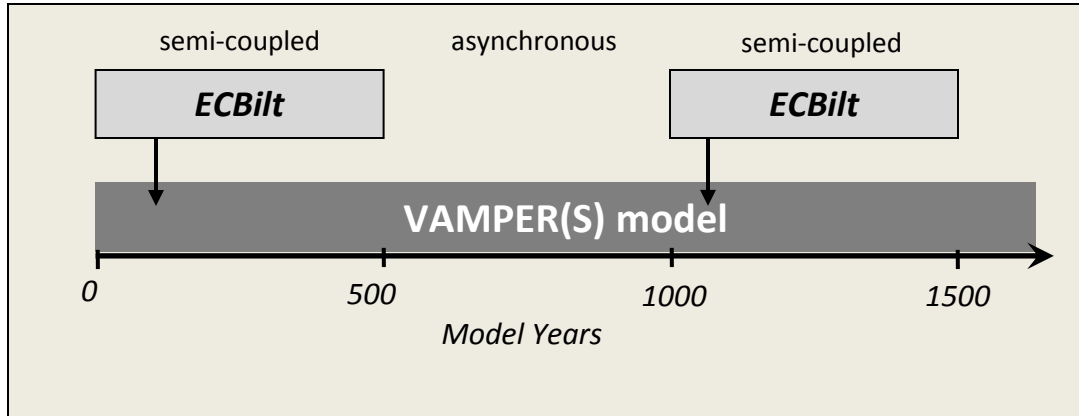
Figure 6. An illustration of asynchronous coupling between VAMPER(S) and ECBilt. The components are run semi-coupled for 100 years while VAMPER(S) is run the entire time. This allows VAMPER(S) to equilibrate with the climate state of *i*LOVECLIM using less computer resources time than a synchronous version.
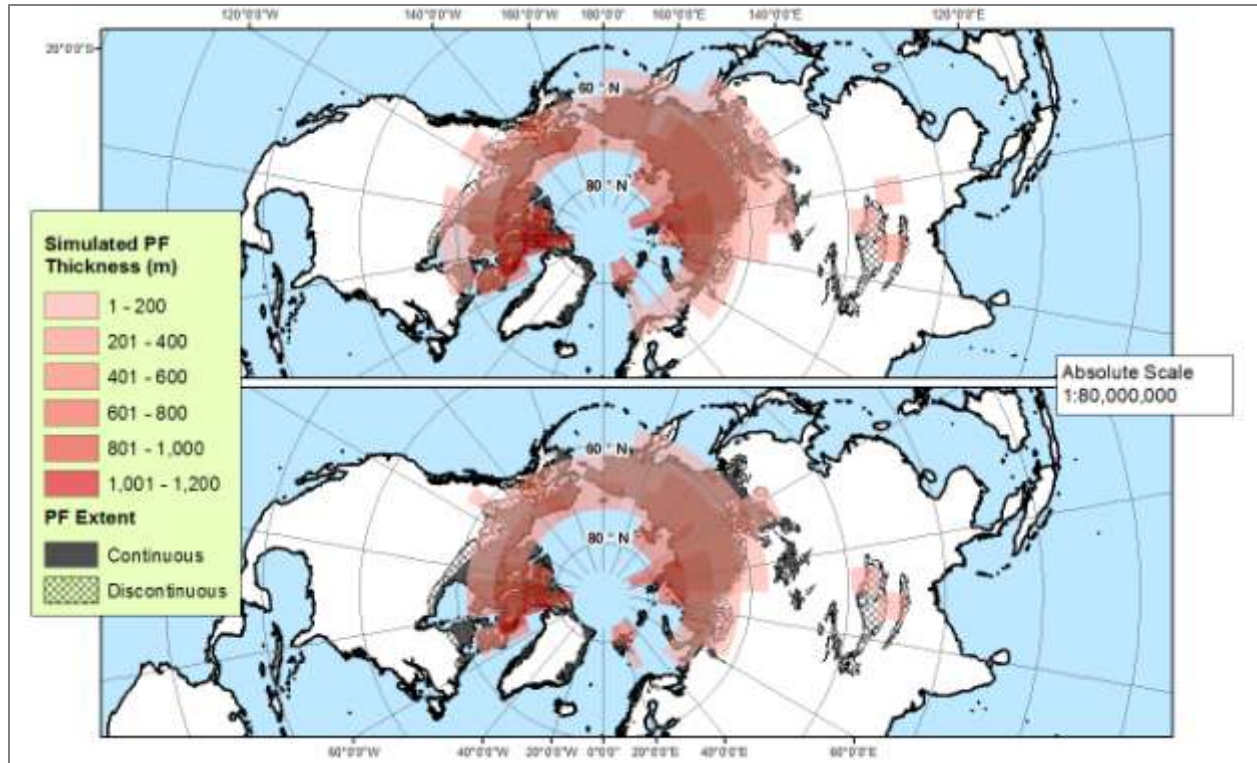
Figure 7. Preindustrial simulation results for permafrost thickness distribution using ECBILT-VAMPER semi-coupling (top) and ECBILT-VAMPER*S* semi-coupling (bottom).
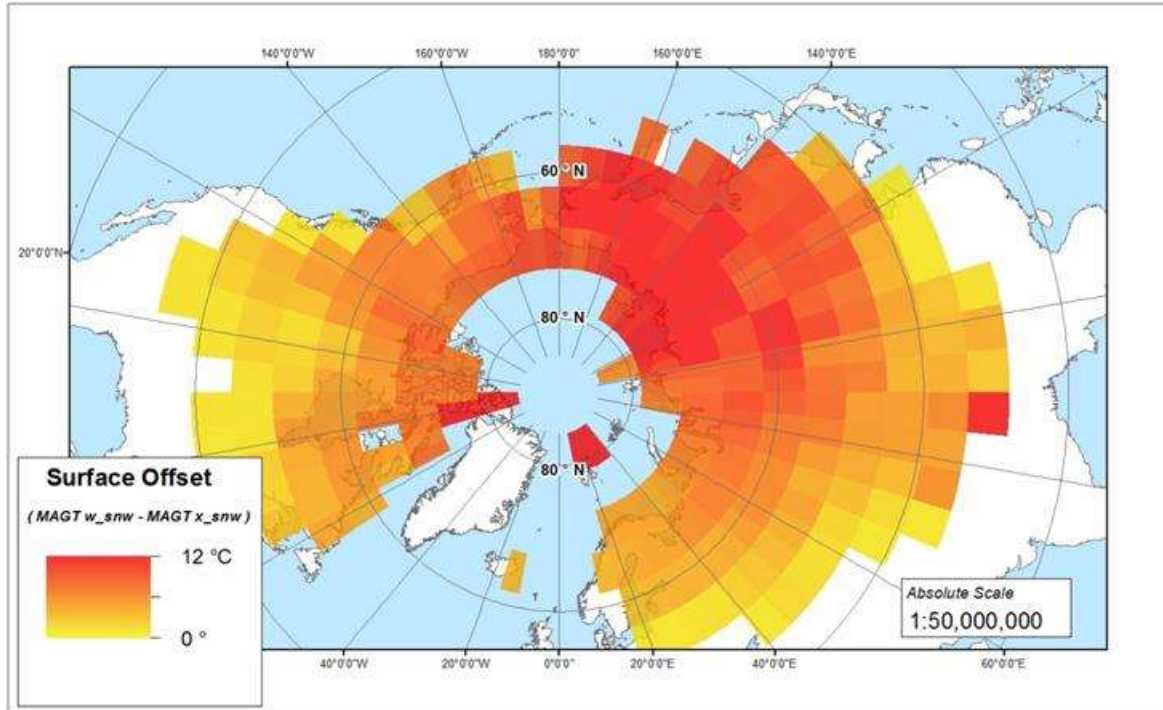
Figure 8. Mean annual surface offset as a result of including the snow option in the ECBilt-VAMPERS coupling.
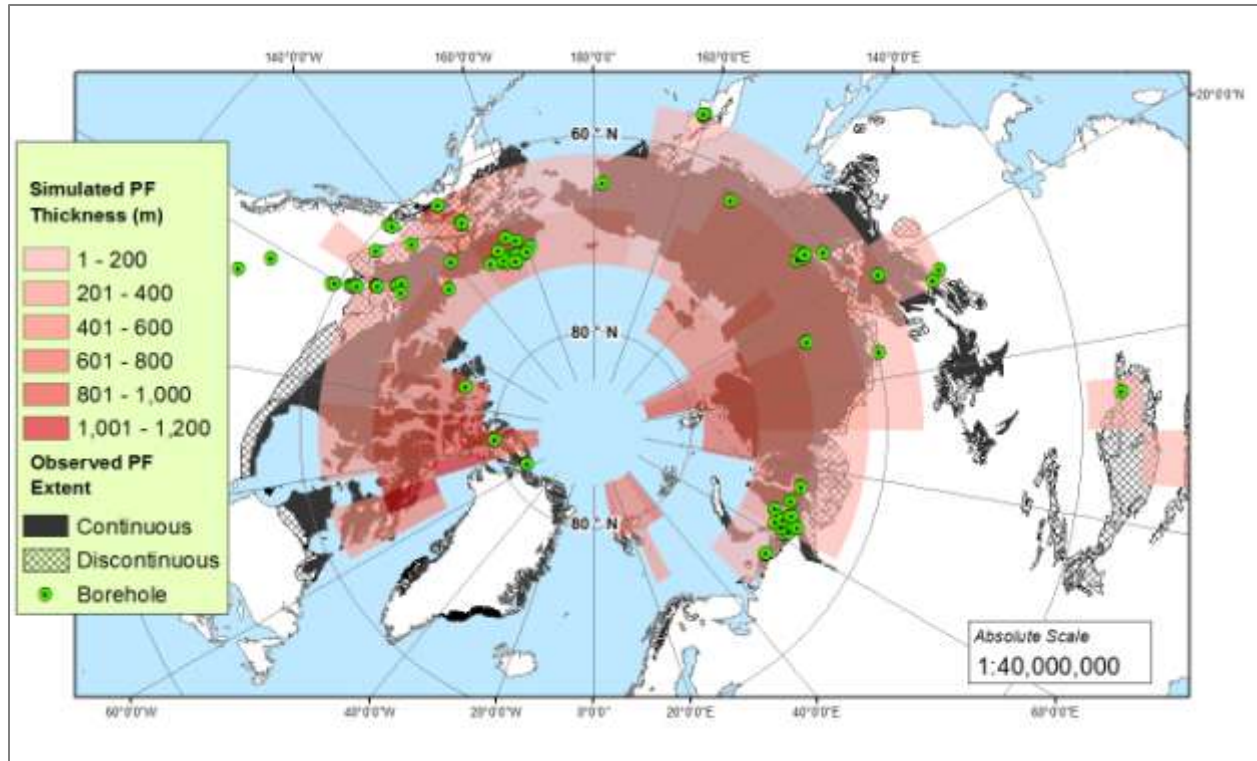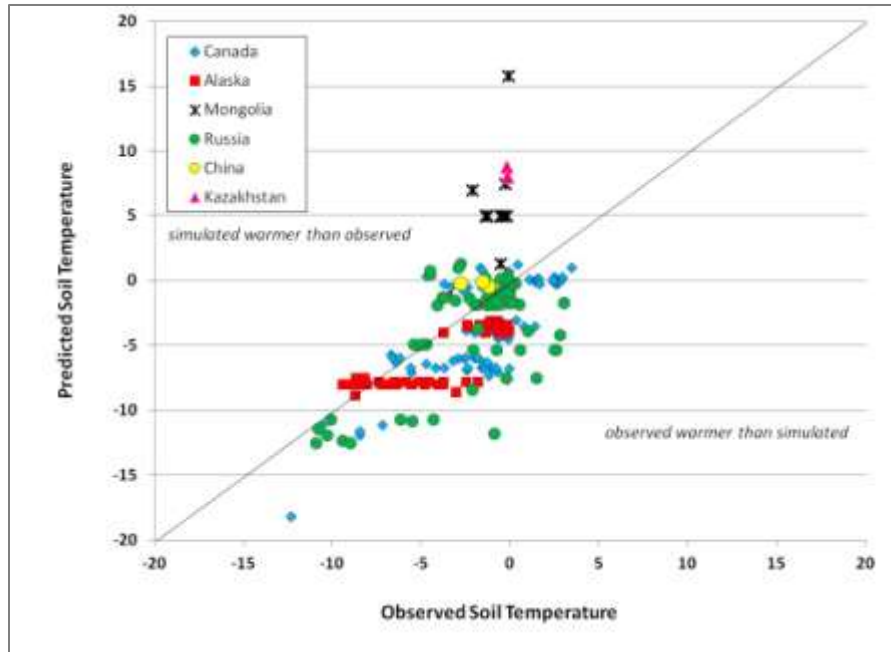
1
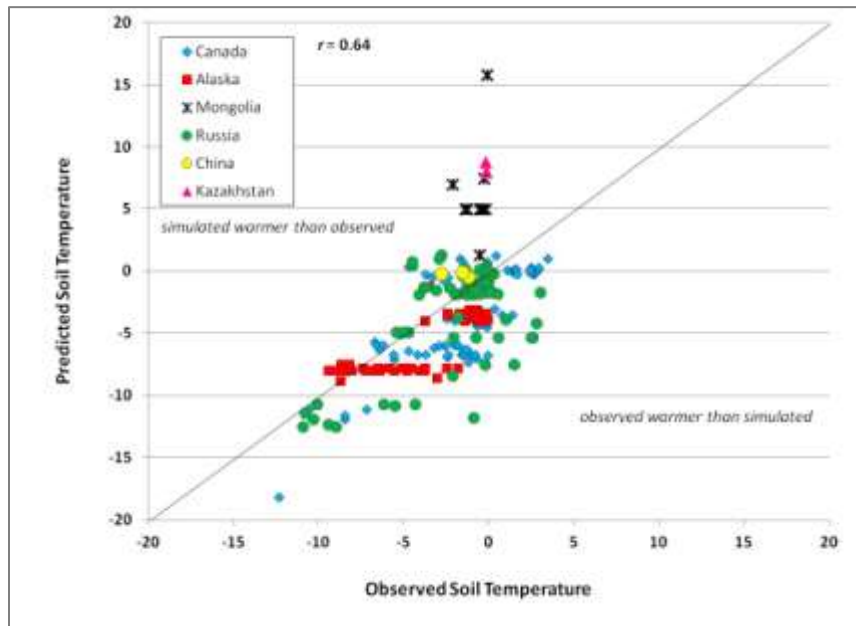
2
3
4 Figure 9. A 1:1 scatterplot comparing simulated thickness results with corresponding permafrost
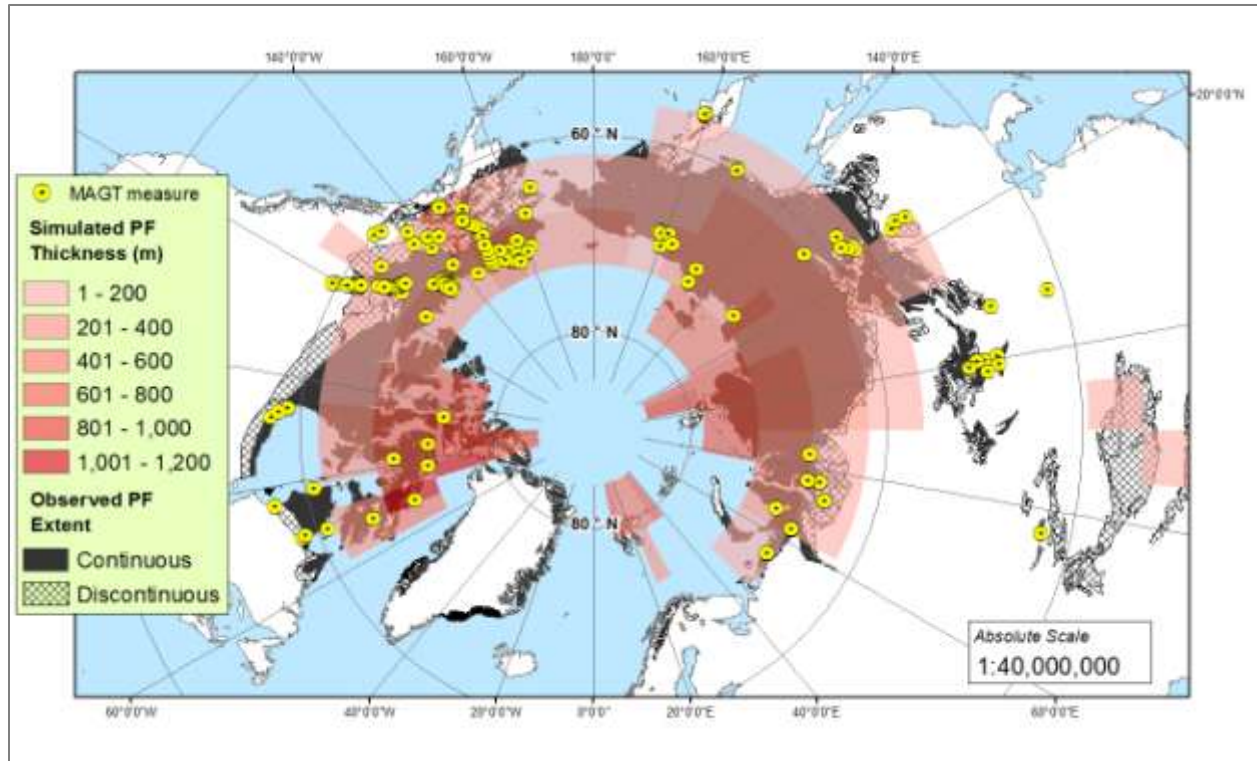5 thickness estimates from borehole data. Points 1-7 are outliers mentioned specifically above.

6

Figure 10. Map of deep GTN-P borehole locations with the simulated permafrost thickness (with snow enhancement) and observed PF extent (Brown et al., 2014).

Figure 11. A 1:1 scatterplot comparing simulated mean annual temperatures with corresponding MAGT measurements.

Figure 12. Map showing locations of the MAGT measurements, collected for the IPY 2010 (GTN-P), used in the comparison to corresponding *i*LOVECLIM simulated subsurface temperatures.